



1 **Six-year source apportionment of submicron organic aerosols from near-**
2 **continuous measurements at SIRTA (Paris area, France)**

3 Yunjiang Zhang^{1,2*}, Olivier Favez^{1*}, Jean-Eudes Petit², Francesco Canonaco³, Francois Truong², Nicolas
4 Bonnaire², Vincent Crenn^{2†}, Tanguy Amodeo¹, Andre S.H. Prévôt³, Jean Sciare^{2,4}, Valerie Gros²,
5 Alexandre Albinet¹

6

7 ¹Institut National de l'Environnement Industriel et des Risques, Verneuil-en-Halatte, France

8 ²Laboratoire des Sciences du Climat et de l'Environnement, CNRS-CEA-UVSQ, IPSL, Université
9 Paris-Saclay, Gif-sur-Yvette, France

10 ³Laboratory of Atmospheric Chemistry, Paul Scherrer Institute, Villigen PSI, Switzerland

11 ⁴Energy, Environment Water Research Centre, The Cyprus Institute, Nicosia, Cyprus

12 [†]Now at ADDAIR, Buc, France

13

14 * Corresponding authors: yjanzhang@gmail.com and olivier.favez@ineris.fr

15

16

17 **Abstract**

18 Organic aerosol (OA) particles are recognized as key factors influencing air quality and climate
19 change. However, highly-time resolved year-round characterizations of their composition and
20 sources in ambient air are still very limited due to challenging continuous observations. Here,
21 we present an analysis of long-term variability of submicron OA using the combination of
22 Aerosol Chemical Speciation Monitor (ACSM) and multi-wavelength aethalometer from
23 November 2011 to March 2018 at a background site of the Paris region (France). Source
24 apportionment of OA was achieved via partially constrained positive matrix factorization (PMF)
25 using the multilinear engine (ME-2). Two primary OA (POA) and two oxygenated OA (OOA)
26 factors were identified and quantified over the entire studied period. POA factors were
27 designated as hydrocarbon-like OA (HOA) and biomass burning OA (BBOA). The latter factor
28 presented a significant seasonality with higher concentrations in winter with significant



29 monthly contributions to OA (18-33%) due to enhanced residential wood burning emissions.
30 HOA mainly originated from traffic emissions but was also influenced by biomass burning in
31 cold periods. OOA factors were distinguished between their less- and more-oxidized fractions
32 (LO-OOA and MO-OOA, respectively). These factors presented distinct seasonal patterns,
33 associated with different atmospheric formation pathways. A pronounced increase of LO-OOA
34 concentrations and contributions (50-66%) was observed in summer, which may be mainly
35 explained by secondary OA (SOA) formation processes involving biogenic gaseous precursors.
36 Conversely high concentrations and OA contributions (32-62%) of MO-OOA during winter and
37 spring seasons were partly associated with anthropogenic emissions and/or long-range
38 transport from northeastern Europe. The contribution of the different OA factors as a function
39 of OA mass loading highlighted the dominant roles of POA during pollution episodes in fall and
40 winter, and of SOA for highest springtime and summertime OA concentrations. Finally, long-
41 term trend analyses indicated a decreasing feature (of about $200 \text{ ng m}^{-3} \text{ yr}^{-1}$) for MO-OOA,
42 very limited or insignificant decreasing trends for primary anthropogenic carbonaceous
43 aerosols (BBOA and HOA, along with the fossil fuel and biomass burning black carbon
44 components), and no trend for LO-OOA over the 6⁺-year investigated period.

45



46 **1 Introduction**

47 Organic aerosol (OA) particles account for a large mass fraction of submicron aerosol (PM_{10}) in
48 the atmosphere (Zhang et al., 2007) and play a key role in regional air pollution and climate
49 (Boucher et al., 2013). OA originates from i) primary emission sources (primary OA, POA),
50 directly emitted into the atmosphere by anthropogenic activities (e.g., fossil-fuel and biomass
51 combustions) or biogenic emissions (e.g., pollen, bacteria, fungal and fern spores, viruses, and
52 fragments of plants), and ii) secondary formation via atmospheric oxidation processes of gas
53 precursors, i.e., biogenic and anthropogenic volatile or semi-volatile organic compounds
54 (VOCs or SVOCs) (Kroll and Seinfeld, 2008; Hallquist et al., 2009; Nozière et al., 2015). Due to
55 their multiplicity and complexity, these various sources and physicochemical mechanisms
56 remain poorly documented and understood. Although numerous time-limited field campaigns
57 allowed to greatly improve our knowledge of OA properties in the last decade (e.g., Jimenez
58 et al., 2009; Lanz et al., 2010; Zhang et al., 2011; Shrivastava et al., 2017; Li et al., 2017;
59 Srivastava et al., 2018a, and references therein), similar studies performed on a multi-year
60 scale remain scarce and particularly challenging (Fröhlich et al., 2015a; Schlag et al., 2016; Sun
61 et al., 2018). Long-term observations and source apportionment of OA are nevertheless
62 necessary to better quantify the contribution of airborne OA particles to air quality and to set-
63 up scientifically-sound emission control strategies. They can also contribute to a better
64 understanding of the atmospheric fate of OA and reduce uncertainties associated with its
65 (in)direct radiative forcing.

66 Online aerosol characterization techniques, such as aerosol mass spectrometry (AMS),
67 have demonstrated their capacity to improve our knowledge of key aerosol chemical
68 components – such as OA - by providing highly time-resolved mass spectral data for the
69 nonrefractory PM_{10} fraction (NR- PM_{10}) (Jayne et al., 2000; Canagaratna et al., 2007). Using
70 receptor model approaches, especially positive matrix factorization (PMF) (Paatero and
71 Tapper, 1994), OA measured by AMS techniques can be further portioned into various source
72 factors using statistic models (Ulbrich et al., 2009; Zhang et al., 2011). For example,
73 hydrocarbon-like OA (HOA) is frequently identified within urban environments and attributed
74 to primary emissions from fuel consumption (Zhang et al., 2007; Jimenez et al., 2009), while
75 biomass burning OA (BBOA) is often resolved specifically during cold seasons or within wild
76 fire plumes (Alfarra et al., 2007; Lanz et al., 2010; Zhou et al., 2017). Oxygenated OA (OOA),



77 commonly considered as a surrogate for SOA, is ubiquitously observed in urban, suburban and
78 remote environments (Zhang et al., 2007; Srivastava et al., 2018a; Zhang et al., 2011; Crippa
79 et al., 2014). OOA can be further separated into different fractions, being for instance
80 classified according to its atmospheric ageing (OOA-type 1 vs. OOA-type 2) or alternatively
81 described as more oxidized (MO-OOA) or less oxidized (LO-OOA) compared to each other
82 (Jimenez et al., 2009; Ng et al., 2011a; Sun et al., 2018). Different OOA factors can also be
83 identified as relevant to various sources of SOA precursors, such as anthropogenic activities
84 (e.g., traffic and biomass burning emissions) (Gilardoni et al., 2016; Gentner et al., 2017) and
85 biogenic emissions (e.g., isoprene and monoterpenes) (Xu et al., 2015; Zhang et al., 2018;
86 Freney et al., 2018) in specific regions and/or seasons. Such source apportionment has the
87 potential to support air quality strategies and shall be able to assess the efficiency of
88 mitigation measures of emission pollutants.

89 Over the last decades, particulate matter (PM) and anthropogenic VOCs emissions in
90 Europe have been drastically reduced in many activity sectors by stringent emission
91 regulations (EMEP, 2016). However, their impacts on both ambient POA and SOA
92 concentrations are poorly assessed and still suffer from the lack of long-term observational
93 data. Based on a less-advanced but more robust technology than AMS, the aerosol chemical
94 speciation monitor (ACSM) has been designed to provide continuous measurements of the
95 main non-refractory chemical species within submicron aerosols (Ng et al., 2011b). As for the
96 AMS, OA mass spectra obtained by the ACSM can be used in PMF analysis for quantification
97 of OA sources (e.g., Sun et al., 2012; Fröhlich et al., 2015b; Zhang et al., 2015). So far, several
98 long-term OA source apportionment studies have been reported based on ACSM
99 measurements at various sites (Canonaco et al., 2015; Fröhlich et al., 2015a; Schlag et al., 2016;
100 Reyes-Villegas et al., 2016; Rattanavaraha et al., 2017; Sun et al., 2018). However, these
101 studies have been limited to periods up to 2-years durations.

102 The longest ACSM timeseries recorded so far (from end of 2011 onwards) is used here
103 to investigate OA sources at a regional background site of the Paris region (France), which is
104 one of the largest urbanized regions in Europe. It has already been demonstrated that OA
105 plays a dominant role in controlling atmospheric pollution in this region (Bressi et al., 2013;
106 Petit et al., 2015). Furthermore, time-limited (typically, 1–2 months) measurement campaigns
107 demonstrated that primary fine aerosols are mainly influenced there by traffic emissions all



108 over the year and residential wood burning during cold seasons, while secondary aerosols
109 originate from both local production and regional transports (Sciare et al., 2011; Crippa et al.,
110 2013a, Crippa et al., 2013b, Petit et al., 2014; Srivastava et al., 2018b). In the present study,
111 main OA factors were identified and quantified from 25 successive and seasonal PMF analyses
112 over 6+ years, with the objective of keeping consistency between these factors from one PMF
113 analysis to another. In this respect, sporadic and/or minor OA sources were not accounted in
114 this study. The seasonal variations, weekly and diel cycles, as well as the long-term temporal
115 trends of the major OA factors were investigated. The relative contributions of the various
116 POA and SOA fractions were also plotted as a function of total submicron OA loadings with
117 the objective to better identify the main OA sources responsible for regional pollution
118 episodes. Finally, the geographical origins of high loadings of SOA factors were investigated
119 using air mass back-trajectory analyses.

120



121 **2 Sampling site and instrumentation**

122 Long-term submicron aerosol on-line measurements used in this study were performed from
123 1st of November 2011 to 26th of March 2018 at the SIRTA facility (Site Instrumental de
124 Recherche par Télédétection Atmosphérique, 2.15 °E, 48.71 °N; <http://sirta.ipsl.fr/>). This
125 exploratory platform is part of the European Aerosols, Clouds, Trace gases Research
126 InfraStructure (ACTRIS, www.actris.eu) (e.g., Pandolfi et al., 2018). It is located 25 km
127 southwest of Paris city center and is considered as representative of the background air quality
128 of the Paris region (Haeffelin et al., 2005; Petit et al., 2015).

129 Major submicron aerosol chemical species i.e., OA, nitrate, sulfate, ammonium, and
130 chloride, were measured using quadrupole ACSM. These measurements were achieved
131 continuously, always using the same instrument, during the investigated period. Data was
132 missing only for a few periods corresponding to two field campaigns performed elsewhere (in
133 fall 2012 and March 2013) and to few technical breakdown and maintenance periods. Detailed
134 descriptions of the ACSM measurement principles and basic data analysis are given by Ng et
135 al. (2011b). Briefly, fine aerosols are sampled into the ACSM system through a 100 mm
136 diameter critical orifice mounted at the inlet of the PM₁ aerodynamic lens (Liu et al., 2007; Ng
137 et al., 2011b). Then, submicron aerosol particles are impacted and vaporized at the
138 temperature (*T*) of about 600 °C and detected using electron impact (70 eV) ionization mass
139 spectrometry. The ACSM was operated at a time resolution of about 30 min with a scan rate
140 of 0.2 s amu⁻¹ from *m/z* 12 to 150 amu (atomic mass unit). Coarse particles were removed
141 upstream using an URG cyclone separator (with the size cut-off diameter of 2.5 μm).
142 Calibrations of the detector response factor were performed regularly (typically every 6
143 months) using ammonium nitrate solutions (Ng et al., 2011b; Freney et al., 2019). The 1.4
144 default value was used for the OA relative ion efficiency for the whole dataset (Canagaratna
145 et al., 2007). The accuracy of these ACSM measurements and the overall good working
146 conditions of the instrument were verified through the participation to the ACTRIS ACSM
147 intercomparison exercises that took place at SIRTA in November - December 2013 and March
148 - April 2016 (Crenn et al., 2015; Fröhlich et al., 2015b, Freney et al., 2019).

149 Co-located multi-wavelength aethalometer (Magee Scientific) datasets were also
150 available for the purpose of the study, providing complementary information on equivalent
151 Black Carbon (eBC) concentrations and sources. Two aethalometers were used successively:



152 from November 2011 to February 2013 (AE31 model) and then from March 2013 to March
153 2018 (AE33 model). Both instruments measure aerosol light attenuation at seven wavelengths,
154 i.e., 370, 470, 520, 590, 660, 880 and 950 nm. The detailed descriptions of the AE31 operation
155 at SIRTA and aethalometer data analysis can be found in Petit et al. (2015). The AE33 is an
156 advanced aethalometer version, which allows better assessment and compensation of the
157 filter-loading effect using two simultaneous light attenuation measurements performed at
158 different rates of particle accumulation onto the filter tape (Drinovec et al., 2015; Drinovec et
159 al., 2017). The mass concentration of equivalent black carbon (eBC) was estimated from
160 attenuation measurement performed at 880 nm as described by Petit et al. (2015) and Zhang
161 et al. (2018). A correction factor of 1.64 was applied to raw absorption data delivered by the
162 instrument as recommended within the ACTRIS network (Zanatta et al., 2016). Furthermore,
163 eBC could be discriminated between its two main combustion sources, i.e., fossil-fuel
164 combustion (eBC_{ff}) and wood burning emissions (eBC_{wb}) using the aethalometer model
165 (Sandradewi et al., 2008; Favez et al., 2010; Sciare et al., 2011; Drinovec et al., 2015). For these
166 calculations, eBC_{ff} and eBC_{wb} were associated with absorption Angström exponents - in the
167 wavelength range 470-950 nm - of 0.9 and 1.7, respectively. These values are also in
168 agreement with a recent study by Zotter et al. (2017).

169 In addition to ACSM and AE33 measurements, co-located off-line analyses were
170 performed from daily (24 h) PM_{2.5} filter samples, collected and analyzed for their content in
171 Elemental and Organic Carbon (OC and EC, respectively) following the ACTRIS
172 recommendations (Zanatta et al., 2017; Zhang et al., 2018). Briefly, filters were collected using
173 a low volume sampler (Partisol Model 2025; Thermo Scientific) equipped upstream with a VOC
174 denuder system. Mass concentrations of OC and EC from August 2012 to March 2018 were
175 then quantified using a Sunset Lab OC/EC analyzer implemented with the EUSAAR-2 thermal-
176 optical protocol (Cavalli et al., 2010). As shown on Figure S1, good agreements were obtained
177 between eBC and EC measurements ($r^2 = 0.79$, slope = 0.94; N=1185 as well as between OA
178 and OC measurements ($r^2 = 0.68$). The slope of 2.14 obtained between submicron OA
179 measured by the ACSM and PM_{2.5} OC filter-based measurements corresponded to the higher
180 range of values generally observed at (sub)urban background sites - typically 1.6-2.2 (e.g., Bae
181 et al., 2006; Aiken et al., 2008; Favez et al., 2010; Sun et al., 2011; Canagaratna et al., 2015
182 and references therein) - and may be partly explained by the fact that the filter sampling set-



183 up has been designed to minimize positive sampling artefacts but do not prevent from
184 negative ones. Results obtained from these comparisons with filter-based measurements
185 supported the validity of the datasets used in the present study.

186 Co-located measurements of nitric oxide (NO) and nitrogen dioxide (NO₂) were
187 performed with a NO₂/NO/NO_x analyzer (model T200UP, Teledyne API, USA). Data
188 measurements were used for further constrain traffic related OA sources. The meteorological
189 parameters, including meteorological parameters including temperature (*T*), relative humidity
190 (RH), wind speed (WS), boundary layer height (BLH), and precipitation were obtained from the
191 main SIRTA ground-based meteorological station, (located at about 4 km North-East of the
192 aerosol monitoring site).

193

194 3. Atmospheric data treatment procedures

195 3.1 PMF analysis

196 Positive Matrix Factorization (PMF) algorithm is a bilinear receptor model (Paatero and
197 Tapper, 1994) which has been widely used in source apportionment of ambient OA measured
198 by AMS or ACSM (e.g., Ulbrich et al., 2009; Zhang et al., 2011; Crippa et al., 2014; Li et al.,
199 2017). As expressed in Eq. (1), observed OA mass spectral matrix (*m/z*-based x_{ij} , dimensions:
200 $m \times n$) can be discriminated into several variables:

$$201 \quad x_{ij} = \sum_{k=1}^p (g_{ik} \cdot f_{kj}) + e_{ij} \quad (1)$$

202 where g_{ik} and f_{kj} refer to factor (source) timeseries and mass spectra profiles, respectively, and
203 e_{ij} correspond to residuals that could not be fitted by the PMF model. In this equation, i and j
204 refer to row (timely resolved ACSM measurement data point) and column (*m/z*) indices in the
205 organic matrix, respectively, while p indicates the number of factors in the PMF solution.
206 Based on a least-squares algorithm, PMF algorithm aims to iteratively minimize residuals and
207 a fit parameter Q , defined in Eq. (2):

$$208 \quad Q = \sum_{i=1}^m \sum_{j=1}^n (e_{ij}/\sigma_{ij})^2 \quad (2)$$



209 where σ_{ij} is the estimated uncertainty of each m/z (j) concentration at each time-step (i) in the
210 so-called error matrix. Organic concentration and error matrices (with m/z ranging from 13 to
211 100) were exported from the ACSM Local software (v 1.5.11.2). Downweighting of the m/z 44-
212 group ions for the PMF model analysis was performed following procedures implemented in
213 the ACSM Local software and following data treatment strategy proposed by Ulbrich et al.
214 (2009).

215 When using PMF, it may be difficult to distinguish between factors with similar spectral
216 profiles, especially for ACSM datasets, which are associated with larger uncertainties
217 compared to AMS (Sun et al., 2012; Zhang et al., 2015; Fröhlich et al., 2015b). The source
218 finder (SoFi) toolkit, implemented with the ME-2 solver (Paatero, 1999), has recently been
219 developed by Canonaco et al. (2013) to better address this limitation. SoFi provides robust
220 functions which allow to constrain chosen factor profiles and/or timeseries. In particular, the
221 so-called α -value approach makes use of range-defining scalar values (with α values ranging
222 from 0 to 1) in order to better elucidate specific PMF factor(s) profile(s) with a chosen degree
223 of freedom; the highest the α -value the less constrained the OA profile (Canonaco et al., 2013).
224 In the present work, this α -value approach has been used to constrain profiles of POA factors.
225 Some previous studies have already been performed at SIRTA using high resolution time-of-
226 flight AMS (HR-ToF-AMS) along with PMF analysis during short-time campaigns (typically
227 around 3-4 weeks), leading to the identification of HOA, BBOA, as well as a cooking OA (COA)
228 factor (Crippa et al., 2013a; Crippa et al., 2013b; Fröhlich et al., 2015b). Mass spectra obtained
229 from these studies were used here as references to constrain POA factors, because of the prior
230 know source information as constraints. Conversely, mass spectral profiles of possible OOA
231 factors were left unconstrained. It should be noted that Crippa et al. (2013c) resolved up to 3
232 different type of OOA factors and/or a marine OA (MOA) factor when combining HR-ToF-AMS
233 and proton-transfer-reaction mass spectrometer (PTR-MS) datasets obtained during a
234 summer and a winter campaign at SIRTA.

235 OOA factor profiles may differ with time, notably due to seasonal variations of a
236 several parameters such as meteorological conditions, photochemistry, atmospheric lifetime,
237 air masses origin, and/or of gaseous precursor origins. In order to better account for such
238 variability, individual PMF analyses were performed on a 3-month basis, i.e., winter
239 (December-January-February), spring (March-April-May), summer (June-July-August), and fall



240 (September-October-November), with a total number of 25 different PMF runs (7 for winters
241 and 6 for each of the other seasons). November 2011 and March 2018 data were included in
242 the winter 2011-2012 and winter 2017-2018 analyses, respectively.

243 To evaluate the influence of the chosen temporal PMF window (i.e., time duration of
244 data used in ME-2 runs) on the seasonal ME-2 model results, different timeframes (i.e., 15, 30,
245 60 and 90 days) were tested. As shown in Figure S2 (with winter 2017 data as an example),
246 the excellent consistency of those results from different scenarios suggest very limited
247 influence of PMF windows on determining the outputs of ME-2 analyses. To better assess the
248 variations in primary and secondary OA in different seasons over the 6⁺-years period and to
249 allow for some degrees of freedom within the model runs, the main OA factors, including both
250 POA factors (HOA and BBOA) and two SOA factors (a less oxidized OOA (LO-OOA) and a more
251 oxidized OOA (MO-OOA)), were calculated as the average of 50 convergent ME-2 runs with a-
252 values varying from 0 to 0.4. Moreover, results obtained with an a-value of 0.2 were also
253 compared to these results for sensitivity analyses (Fig. S3). The diagnostics of the final OA-
254 factor solution are further discussed in section 4.1.

255

256 3.2 Influence of biogenic SOA

257 Biogenic SOA (BSOA) might have a significant influence on OA loadings in mid-latitude regions
258 during summertime and be further apportioned using AMS techniques (e.g., Leaitch et al.,
259 2011; Canonaco et al., 2015). For that reason, influence of this biogenic OA source was
260 specifically investigated in the present study. To do so, BSOA derived from terpene emissions
261 (BSOA_t) was taken as a surrogate for total BSOA and the temperature (*T*) dependence of the
262 BSOA_t formation process yield during summertime was simulated using a simple terpene
263 emission model (Goldstein et al., 2009; Schurgers et al., 2009; Leaitch et al., 2011 and
264 references therein), where an exponential curve function is describing the relation between
265 terpene emission rate (γ) and the air *T*, following Eq. 3:

$$266 \quad \gamma = \gamma_0 \times e^{\beta(T-303)} \quad (3)$$

267 where γ_0 stands for the emission rate ($\mu\text{g g}^{-1} \text{h}^{-1}$) at standard conditions, and β is an empirical
268 constant chosen here to be equal to 0.09 K⁻¹ (Schurgers et al., 2009; Leaitch et al., 2011). As



269 reported by previous studies, biogenic terpene emissions could be a major source of such PMF
270 LO-OOA factor observed during summertime in western Europe (e.g., Canonaco et al., 2015;
271 Daellenbach et al., 2017; Daellenbach et al., 2019). Given that, $BSOA_t$ was assumed to be
272 mainly included in the LO-OOA fraction in the present work, and $BSOA_t$ estimated
273 concentrations were compared to LO-OOA concentrations data points corresponding to the
274 daytime maximum T (at approximately 16:00 – 17:00 local time) in summer. Assuming that
275 LO-OOA could actually be mostly composed of $BSOA_t$ during this period of the day and
276 following the procedure described by Leaitch et al. (2011), the daily mass concentrations of
277 $BSOA_t$ were estimated as follows:

$$278 \quad BSOA_{t,estimated} = LO - OOA_{(observed\ at\ T_{min})} \times \frac{\gamma}{\gamma(T_{min})} \quad (4)$$

279 where T_{min} corresponds to the lowest daily maximum T observed across the investigated
280 summer seasons (i.e., $12^\circ\text{C} \pm 1^\circ\text{C}$) and $LO-OOA_{(observed\ at\ T_{min})}$ corresponds to the mean LO-OOA
281 concentration obtained for these data points ($0.7 \pm 0.3 \mu\text{g m}^{-3}$, $N = 17$).

282

283 3.3 Trend analysis

284 The multi-year trends of OA factors obtained from the ME-2 analysis were analyzed using the
285 Mann-Kendall (MK) trend test. The MK test is a nonparametric test for monotonic trend in a
286 timeseries (Mann, 1945). The MK test is better suitable for nonnormally distributed, censored
287 and missing data, compared to parametric statistical tests, such as the t test. The normality of
288 the mass concentrations of the OA factors was examined by the Shapiro-Wilk normality test
289 (Shapiro and Wilk, 1965). As a result of the Shapiro-Wilk normality test, all datasets of the
290 mass concentrations of the four OA factors were not normally distributed cases. The MK test
291 associated with Sen's estimator of slope (Sen, 1968) is insensitive to outliers, while it is not
292 appropriate for the chosen dataset with significant seasonality. Thus, the seasonal MK test
293 was used for the trend analysis when observed data had a significant seasonality with the
294 Kruskal-Wallis test (Kruskal and Wallis, 1952). The trend computation was performed here
295 using a R trend package (Pohlert, 2018). We applied monthly average data for all those tests
296 to illustrate the smoothed structure.

297



298 3.4 Air mass back-trajectory analysis

299 The HYbrid Single Particle Lagrangian Integrated Trajectory model (Hysplit) Draxler and Rolph,
300 2003; Stein et al., 2015) was applied to calculate 72-h back trajectories hourly arriving at SIRTA
301 at a height of 100 m above ground level, based on GDAS meteorological data. The potential
302 source contribution function model (PSCF) (Polissar et al., 1999) was used in this study to
303 investigate the potential source origins that may contribute to high concentrations of OA
304 factors at SIRTA. This analysis was achieved with a resolution of $0.2^\circ \times 0.2^\circ$ for each grid cell,
305 using the ZeFir toolkit (Petit et al., 2017). The probability function for a given grid cell (i, j),
306 where i stands for the latitude and j for the longitude, is related to observed concentrations
307 that are higher than a threshold value, which is defined by Eq. (6):

$$308 \quad PSCF_{(i,j)} = \left(\frac{m_{ij}}{n_{ij}} \right) \cdot w_{ij} \quad (6)$$

309 where m_{ij} is the total number of selected trajectory endpoints (i, j) associated with receptor
310 concentrations of PMF factors higher than the threshold value, and n_{ij} is the total number of
311 back trajectory endpoints at each grid cell (i, j). The 75th percentile of each OA factors during
312 the entire study was used as the threshold value to calculate m_{ij} . To reduce uncertainty caused
313 by small n_{ij} values for the PSCF modelling, an arbitrary weighting function (w_{ij}) was applied
314 using Eq. (7) (Waked et al., 2014). To minimize the influence of some trajectories on the
315 possible pathways of air mass transport, observed data points associated with low wind speed
316 conditions ($WS < 4 \text{ m s}^{-1}$) were filtered out. In addition, observed data points at SIRTA during
317 the period with any hourly precipitation events (precipitation $> 0 \text{ mm}$) were removed to
318 reduce influence of wet deposition on ambient aerosol concentrations.

$$319 \quad w_{ij} = \begin{cases} 1 & \text{for } \log(n_{ij} + 1) \geq 0.85 \max \log(n_{ij} + 1) \\ 0.725 & \text{for } 0.6 \max \log(n_{ij} + 1) \leq \log(n_{ij} + 1) < 0.85 \max \log(n_{ij} + 1) \\ 0.475 & \text{for } 0.35 \max \log(n_{ij} + 1) \leq \log(n_{ij} + 1) < 0.6 \max \log(n_{ij} + 1) \\ 0.175 & \text{for } \log(n_{ij} + 1) < 0.35 \max \log(n_{ij} + 1) \end{cases} \quad (7)$$

320

321 4 Results and discussion

322 4.1 Identification of the main OA factors



323 **4.1.1 Determination of the optimum factor number**

324 The optimal number of PMF OA factors shall be determined by the distribution of the
325 main sources at a given sampling site. Based on results obtained from the compilation of
326 previous AMS studies reported in the Paris region, two POA factors - HOA and BBOA - and two
327 OOA fractions - MO-OOA and LO-OOA – are undoubtedly major fraction of submicron aerosols
328 in Paris area over the year (Crippa et al., 2013a; Crippa et al., 2013b; Freutel et al., 2013; Petit
329 et al., 2014; Fröhlich et al., 2015b). Another POA source, i.e., COA, has also been identified
330 using HR-ToF-AMS during previous campaigns in Paris region (Crippa et al., 2013a; Crippa et
331 al., 2013b; Fröhlich et al., 2015b). However, the distinction between COA and HOA factors
332 based solely on ACSM measurements remains challenging due to highly similar mass spectra
333 and uncertainties associated with the ACSM low mass spectral resolution (Petit et al., 2014;
334 Fröhlich et al., 2015b).

335 To better assess a potential role of COA in our source apportionment study, several
336 ME-2 runs were conducted constraining either three POA factors (HOA, BBOA, COA) or two
337 (HOA, BBOA). In these tests, POA reference mass spectra determined by Fröhlich et al. (2015b)
338 were employed as anchor profiles (with α -values ranging from 0 to 0.4 with steps of 0.05).
339 PMF solutions with a factor number ranging from 3 to 6 were investigated on ACSM datasets
340 corresponding to different seasons of different years (December 2011 - February 2012, March
341 - May 2015, June - August 2017, September - November. 2017, December 2017 - February
342 2018). Results obtained from these preliminary individual PMF runs showed very good
343 consistency between them with two unconstrained OOA factors - MO-OOA and LO-OOA -
344 always appearing in the 4-factor (with constrained HOA and BBOA factor) and 5-factor (with
345 constrained HOA, BBOA and COA factor) solutions. Conversely, 3- and 6-factor PMF analyses
346 generally led to unsatisfactory solutions.

347 Figures 1 and S4 present results obtained for the 4- and 5-factor solutions, respectively,
348 for the winter 2017-2018 period, taken here as an example. In both cases, mass spectra were
349 in good agreement with those reported in the literature. However, the COA and BBOA factors
350 are displaying very similar diel patterns, leading to surprisingly good correlations between
351 these two factors (see Figure S5). It could then be concluded that COA-like aerosols at SIRT
352 were primarily linked with wood burning emissions and pure cooking aerosols were probably
353 present in too low loadings to be properly quantified within the present study. This



354 assumption is consistent with conclusions drawn by other studies performed at SIRTA (Petit
355 et al., 2014; Srivastava et al., accepted for publication) as well as other studies showing that
356 the COA factor could not be solely attributed to cooking aerosols (e.g., Freutel et al., 2013,
357 Dall'Osto et al., 2015).

358 Therefore, the 4-factor solution, including two constrained POA factors (BBOA and
359 HOA) and two unconstrained factors, was chosen here as the “best estimate” for the PMF
360 runs performed over the long-term dataset. A total of 25 seasonal and individual PMF analyses
361 were then conducted using a similar procedure. The seasonal OOA factor mass spectra are
362 presented in Figure S6, showing high seasonal consistency for each OA factor. Moreover, as
363 shown in Figure S7, the distribution of residuals derived from the these 4-factor solution ME-
364 2 runs was sharply centered around 0, suggesting insignificance of possible unresolved OA
365 factor(s).

366

367 **4.1.2 Source attribution**

368 BBOA mass spectra are quite constant throughout the seasons, and present
369 characteristic peaks at m/z 29, 60, and 73 indicative of biomass burning combustion (Figure
370 S6). As shown on Figure 2a, BBOA diel cycles displayed well-marked patterns with strong
371 nighttime maxima, especially during the weekend. This confirms the predominance of
372 residential wood burning activities on BBOA concentrations at SIRTA and in the Paris region,
373 as already shown previously (e.g., Favez et al., 2009; Sciare et al., 2011; Crippa et al., 2013b;
374 Petit et al., 2014). As expected, BBOA diel cycles are similar to the ones obtained for eBC_{wb} ,
375 except for small eBC_{wb} morning peaks that were not observed for BBOA (possibly due to
376 uncertainties of the aethalometer model) and for lunch-time shouldering within BBOA
377 patterns, which might be related to limited COA emissions (see above). Interestingly, both of
378 this eBC_{wb} and BBOA daytime rises were not observed during week-end, suggesting the
379 influence of local emissions related to working activities (e.g., eBC from commuting road
380 transport and staff canteens).

381 Compared to BBOA, HOA shows a more complex weekly diel pattern (Figure 2b). Its
382 pattern is generally similar to eBC_{wb} and NO_x (both being considered here as markers for traffic
383 emissions). HOA presents two peaks during working day, one in the morning and another in



384 the evening. Morning peaks, occurring during traffic rush hours are clearly indicative of road
385 transport contributions, confirming HOA as a proxy for traffic emissions. However, HOA
386 evening peaks occurs globally later than eBC_{ff} and NO_x ones (9:00-10:00 PM vs. 7:00 PM,
387 respectively) and much lower ratio are observed between HOA and eBC_{ff} in the morning than
388 in the evening. This might be partly explained by i) higher eBC traffic emission factor in the
389 morning and/or ii) impacts of biomass burning sources on HOA concentrations in the late
390 evening. Moreover, eBC_{ff} shows a clear weekend effect, with less-pronounced pattern on
391 Saturday and Sunday due to road transport reduction, while HOA displays intense nighttime
392 peaks during weekend. This HOA mean pattern was substantially influenced by winter data,
393 whereas summertime patterns display better consistency between HOA, eBC_{ff} and NO_x (Figure
394 S8). Altogether, these results claimed for considering HOA as a mixed factor partly composed
395 of traffic and biomass burning aerosols. This statement is in good agreement with conclusions
396 from complementary studies showing wood burning contribution to HOA at the same site
397 (Petit et al., 2014; Srivastava et al., accepted for publication). It was further supported by
398 higher *m/z* 44 contribution within HOA mass spectra in fall and winter than during the spring
399 and summer seasons (Figure S6), which could be characteristic of the presence of processed
400 biomass burning emissions (e.g., Grieshop et al., 2009; Fröhlich et al., 2015b).

401 As presented in Figures 1 and S6, MO-OOA mass spectra present a strong peak at *m/z*
402 44. In fact, this spectrum has been widely reported as low volatility OOA (LV-OOA) and
403 considered as composed of highly oxidized and aged SOA (Lanz et al., 2007; Ulbrich et al., 2009;
404 Zhang et al., 2011; Ng et al., 2011a). Compared to the poorly pronounced diel variability of
405 sulfate, this MO-OOA factor exhibits a slight enhancement at nighttime (Figure 2c), suggesting
406 a possible local formation mechanism involving nighttime chemistry, on top of its overall
407 regional feature. The geographic origins of the MO-OOA factor are further discussed in section
408 4.2.1 for each season.

409 The mass spectra of LO-OOA in this study present a higher *m/z* 43 and a lower *m/z* 44
410 (Figures 1a and S6), compared to MO-OOA, which is consistent with the mass spectral pattern
411 of previously reported freshly-formed semi-volatile OOA (SV-OOA) (Jimenez et al., 2009; Ng
412 et al., 2010). The diel variations of LO-OOA display higher concentrations during nighttime
413 than daytime (Figure 2d), with relative variations much more pronounced than for the MO-
414 OOA diel pattern. These results support different formation pathways of the two OOA



415 fractions. In winter, LO-OOA mass spectra has higher contributions of m/z 29 as well as
416 elevated m/z , i.e., starting from m/z 60, than during other seasons (Figure S6). Such
417 characteristics suggest a major influence of biomass burning emissions onto the LO-OOA
418 factor during wintertime, as previously proposed from measurements at SIRTA (e.g., Crippa et
419 al., 2013c). Conversely, in summer, this factor may be significantly influenced by BSOA
420 formation (Canonaco et al., 2015; Daellenbach et al., 2017). To investigate this possible origin,
421 we checked if summertime LO-OOA concentrations at higher daily T were following
422 temperature dependence similar to the one expected for the formation of terpene SOA, as
423 explained in section 3.2. Results of these calculations are presented in Figure 3. LO-OOA
424 concentrations substantially increase with T , showing a good agreement with the estimated
425 BSOA_t formation exponential profiles. However, when comparing with estimation derived
426 from Eq. (4) (referred to Figure 3), observed LO-OOA displays substantially higher loadings
427 than estimated BSOA_t at highest concentration range. This could be partly due to the influence
428 of regional transports and atmospheric dilution on aerosol loadings and some possible
429 uncertainties (such as unclear formation schemes of biogenic SOA at SIRTA), which were not
430 considered in the BSOA_t estimation. These comparison results between observation and
431 estimation indicates that the LO-OOA factor observed in summer might be mainly associated
432 with biogenic sources. This was aligned with the VOC seasonal patterns observed in the Paris
433 region (Baudic et al., 2016), although the underlying SOA formation mechanism is still unclear
434 and needs to be further investigated (Beekmann et al. 2015).

435

436 **4.2 OA factor temporal variations**

437 Figure 4 presents timeseries of total submicron OA and its four main factor components
438 (namely HOA, BBOA, MO-OOA and LO-OOA) together with key meteorological parameters:
439 boundary Layer height (BLH), relative humidity (RH) and temperature (T), during the entire
440 investigated period. Most meteorological parameters present seasonal cycles. For example,
441 the highest and lowest air T were observed during summertime and wintertime, respectively,
442 while the highest RH was frequently observed in winter for each year. The highest BLH was
443 mainly observed in summer among all seasons. Total submicron OA presented dynamic
444 variations during all seasons with hourly average concentrations ranging from 0.03 to 77.5 μg
445 m^{-3} and daily average values from 0.2 to 41.3 $\mu\text{g} \text{m}^{-3}$. There was no clear seasonality for the



446 total monthly average OA concentrations, varying from 4.8 to 5.1 $\mu\text{g m}^{-3}$. However, each
447 individual OA factors displayed intra and inter-annual variations, which are discussed in this
448 section.

449

450 **4.2.1. Monthly and seasonal variations of OA factors**

451 Figure 5 illustrates monthly average concentrations obtained for each OA factor over the
452 studied period. HOA monthly concentrations vary from 0.4 to 1.3 $\mu\text{g m}^{-3}$ and display a
453 statistically insignificant seasonal trend ($p > 0.05$, Figure 5a). Nevertheless, the mass
454 concentration of HOA is nearly twice higher during cold months (in the range of 0.9 – 1.3 $\mu\text{g m}^{-3}$
455 m^{-3} , from November to March) than in other months (in the range of 0.4 – 0.5 $\mu\text{g m}^{-3}$ from
456 April to October). This monthly cycle of HOA could be partially explained by lower BLH
457 conditions and influence of more intense emissions of biomass burning in cold seasons than
458 in warm seasons (Figures 4 and S9). As illustrated by Figure S10, HOA clearly presents two
459 peaks (in the morning and late evening) for each season. The evening HOA peak is significantly
460 higher than the morning peak in winter and fall seasons when high loadings of BBOA are
461 observed as well. Although dynamic processes (establishment of a stable nighttime boundary
462 layer) cannot be excluded, these results point to a possible contribution of biomass burning
463 emissions to the HOA factor in the evening during cold months, as discussed before from the
464 diel cycles of OA factors.

465 As shown in Figure 5b, BBOA displays a statistically significant seasonal pattern trend
466 ($p < 0.0001$) with higher monthly mean concentrations (1.1 – 1.9 $\mu\text{g m}^{-3}$) during cold months
467 (November – March) than during the April – September period (0.3 – 0.5 $\mu\text{g m}^{-3}$). This seasonal
468 dependence of wood burning emissions is associated with the residential heating activities
469 over the Paris region. BBOA presents a seasonal dependence of its diel cycle, as presented in
470 Figure S10. In particular, BBOA shows an evident peak at evening/nighttime in winter, spring,
471 and fall, while it presents a stable diel cycle during summertime. The highest seasonally-
472 averaged nighttime peak (up to 2.4 $\mu\text{g m}^{-3}$) is observed in winter, highlighting a significant
473 enhancement of wood burning emissions and influence of meteorological conditions (such as
474 low BLH) during this season.



475 Monthly average mass concentrations of MO-OOA present a significant seasonal trend
476 ($p < 0.05$), varying from 1.0 in September to 3.5 $\mu\text{g m}^{-3}$ in March (Figure 4c), in agreement with
477 previous studies performed in Europe (Schlag et al., 2016; Daellenbach et al., 2017; Bozzetti
478 et al., 2017). The highest MO-OOA mass concentrations observed in the cold months are
479 somehow similar to the seasonal variation of BBOA. MO-OOA diel cycles also present a
480 seasonal variation, with significant increase during evening/nighttime in winter, spring, and
481 fall (Figure S10). In order to minimize the effect of atmospheric dilution and regional transport,
482 the mass concentration of MO-OOA was normalized to sulfate, the latter one being considered
483 as a regional secondary production marker (Petit et al., 2015 and Figure S11). As shown in
484 Figure S11, the correlations between MO-OOA and sulfate are found to be strongly BBOA- and
485 wind speed-dependent. For high wind speed and low BBOA concentrations, the mean MO-
486 OOA-to-sulfate ratio is close to 1, while it reaches up to 8 under high BBOA and low-to-medium
487 wind speed. This is consistent with the assumption of an enhancement of MO-OOA formation
488 in the presence of substantial biomass burning emissions, which have been reported as a
489 major anthropogenic SOA source (Heringa et al., 2011; Tiitta et al., 2016; Bertrand et al., 2017).
490 Furthermore, high concentrations of MO-OOA are generally observed at high RH ($> 80\%$) and
491 low T ($< 0\text{ }^{\circ}\text{C}$) conditions during wintertime (Figure S12) and the MO-OOA-to-sulfate ratio
492 shows a significant enhancement as a function of RH (Figure S13), suggesting that the
493 aqueous-phase heterogeneous processes may represent an important pathway for the local
494 MO-OOA formation in winter as proposed by Gilardoni et al. (2016). Conversely, there are no
495 obvious RH- T dependent patterns for the MO-OOA in spring (Figure S12), indicative of more
496 complex formation processes during this season. In summer, MO-OOA displays evident
497 increase from early afternoon to evening (Figure S10), suggesting significant local
498 photochemical production of SOA particles in summer with higher T and increased solar
499 radiation (Petit et al., 2015). As a matter of fact, MO-OOA presents high concentrations under
500 high T ($> 25\text{ }^{\circ}\text{C}$) and low RH ($< 65\%$) summertime conditions (Figure S12). In conclusion, and
501 despite relatively constant mass spectra all over the year, MO-OOA appears to originate from
502 various seasonal-dependent formation pathways and sources (such as biomass burning and
503 biogenic sources), that should still be investigated in more details.

504 The LO-OOA mass spectra with high f_{43} / f_{44} ratios are frequently observed in spring,
505 summer and fall, whereas a lower ratio is obtained for winter (Figure S6). These different mass



506 spectra of LO-OOA could be partially explained by seasonal-dependent formation mechanisms
507 and sources. The monthly mean mass concentrations of LO-OOA vary from 0.8 to 3.6 $\mu\text{g m}^{-3}$
508 (Figure 5d) and shows a statistically significant seasonality ($p < 0.001$) with higher
509 concentrations during warm months and lower during cold months. As discussed above, the
510 highest summertime LO-OOA concentrations are assessed to be mainly linked with BSOA
511 formation. As presented in Figure S12, T -RH dependence of the LO-OOA factor is very different
512 according to the season. In particular, the highest wintertime LO-OOA concentrations are
513 mainly observed at low T and high RH conditions, suggesting that gas-particle partitioning may
514 play an important role in LO-OOA formation during this season. In summer, the LO-OOA
515 concentrations present strong T positive dependence while RH dependence is not clear,
516 indicating that photochemical production of LO-OOA became more important in summer than
517 in winter. Moreover, high concentrations of LO-OOA are observed at daytime in summer,
518 which is different from the diel variations in other seasons with high concentrations only
519 during nighttime (Figure S10). Such LO-OOA diel variations could further support the
520 photochemical processing dominating the LO-OOA production in summer.

521

522 4.2.2. Long-term trends

523 Figure 6 presents the results obtained from the trend analysis of the 6-year timeseries of the
524 four OA factors as well as eBC_{ff} and eBC_{wb} components. The significance and magnitude of
525 these trends were examined using the MK p -value and Sen's slope, respectively. BBOA
526 presents a statistically significant decreasing trend ($p < 0.05$) with a Sen's slope of about 80 ng
527 m^{-3} per year in the Paris region. On the other hand, eBC_{wb} concentration trends appear quite
528 stable over the investigated period. Two possible reasons may explain the discrepancy trend
529 results between BBOA and eBC_{wb} . It may be hypothesized that a limited overall improvement
530 of wood stove performances in the Paris region could have influence BBOA emission factors
531 more than eBC_{wb} ones, but no evidence has been found to support this assumption. Similarly,
532 but in the opposite way, eBC_{ff} was found to have a significant decreasing trend, while HOA
533 trend was found to be statistically insignificant (p -value > 0.05). However, if removing the high
534 concentration peak observed in December (for which an important contribution of wood
535 burning HOA can be expected), the MK p -value is reduced to be 0.024, which would be
536 indicative of a significant decreasing trend (with a related Sen's slope of 72 ng m^{-3} per year).



537 These results would be in line with a reduction of PM traffic emissions over the past years in
538 France, as estimated by the French emission inventory state operator (CITEPA, 2018).
539 However, such trends analysis should be performed on longer datasets for a much better
540 evaluation of the pollution control strategies (both on road transport and residential heating
541 emissions) in the Paris region.

542 MO-OOA shows a significant decreasing trend ($p < 0.05$) with a Sen's slope of 204 ng
543 m^{-3} per year. Considering the overwhelming secondary origin of this factor, this significant
544 decreasing trend may be partially explained by a reduction of anthropogenic VOCs emissions
545 in France over the investigated period (CITEPA, 2018). LO-OOA presents no significant trend
546 (with $p = 0.29$). As discussed above, higher LO-OOA loadings may be linked to BSOA formation,
547 especially at summertime. The stability of LO-OOA concentrations over time may be linked to
548 limited changes in biogenic VOC emissions and/or in relevant oxidant concentrations, that
549 control the SOA burden in the atmosphere. Effect of anthropogenic-biogenic interaction
550 mechanisms on biogenic SOA formation - e.g., involving NO_x , as reported by previous studies
551 in urban regions (Budisulistiorini et al., 2015; Zhang et al., 2017) - could also partially explain
552 the limited changes for the long-term trend of LO-OOA at SIRTA. Detailed LO-OOA formation
553 processes involved here still need to be further investigated. Nevertheless, it may be assumed
554 that reductions of anthropogenic VOC emissions only cannot be sufficient to weaken the total
555 SOA background concentrations in the Paris area.

556

557 **4.3 OA source contribution as a function of OA concentrations**

558 Figure 7 presents the contribution of the four OA sources as a function of total submicron OA
559 mass loadings or each season along with percent changes of meteorological conditions. In
560 winter and fall, all meteorological parameters - except limited changes in RH - show negative
561 relationships as a function of the OA mass concentrations, confirming the coincidence of low
562 T , low WS, and/or low BLH in the formation of pollution episodes (Dupont et al., 2016). POA
563 contributions gradually increase with increasing OA concentrations: an OA increase from
564 below $5 \mu\text{g m}^{-3}$ to above $25 \mu\text{g m}^{-3}$ leads to a POA contribution increase from 35 % (resp. 27 %)
565 up to 64 % (resp. 70 %) in winter (resp. fall). These results illustrate the major role of primary
566 sources during periods with high OA concentrations during the cold seasons. In particular,



567 BBOA contribution gradually increase from 21 % (15 %) to 41 % (40 %) in winter (fall) along
568 with OA mass loading increase.

569 In spring, OA composition is radically changed and is dominated by the two OOA
570 fractions, with almost constant average contributions (68 – 77%) regardless OA concentration
571 levels, indicating the major role of SOA during this season. MO-OOA presents higher
572 contributions to OA (45-53%) than LO-OOA (15-31%), suggesting that the formation of aged
573 SOA plays a key role on the build-up of episodes with high OA concentrations during
574 springtime. As shown in Figure 8f, the percent changes in *T*, WS, and BLH gradually decrease
575 with increasing OA concentrations. By contrast, RH shows a positive relationship with OA mass
576 concentrations, with the largest RH enhancement (16%) at highest OA-loading bin ($> 25 \mu\text{g m}^{-3}$).
577 This may suggest that high RH being the most favorable environment condition for SOA
578 formation during springtime OA pollution episodes, as supported by a high contribution of
579 OOA factors at the highest OA concentration level (Figure 7b). In addition, although BBOA
580 contributions remained relatively limited, it increases from 11% to 17% when OA increased
581 from less than $10 \mu\text{g m}^{-3}$ to $> 25 \mu\text{g m}^{-3}$. This may reveal a non-negligible influence of wood
582 burning emissions during early spring pollution episodes.

583 In summer, OA was also dominated by the two OOA fractions (around 80-85% at all
584 OA-loading bins). The LO-OOA contribution gradually increase from 51 % to 69% as a function
585 of OA mass loadings associated with a significant increase of *T*. Other meteorological variables
586 (i.e., RH, WS and BLH) showed relatively stable changes across different OA mass loadings
587 (Figure 7h). These results confirm that high OA concentrations during summer are strongly
588 determined by *T*-driven biogenic SOA formation processes.

589

590 **4.4 Potential geographic origins of SOA factors**

591 Figure 8 shows maps of the most probable geographic origins of the two OOA factors for each
592 season based on PSCF analysis. In winter, MO-OOA presents high PSCF values over the Benelux,
593 Germany and Poland, showing a major influence of long-range transport of OA from
594 northeastern sectors. Similar results are obtained from wind-dependent analyses (Figure S14).
595 This could be associated with more stable conditions with anticyclonic conditions, but could
596 also suggest more intense SOA production and aging processes at regional scale for



597 continental air masses. As a matter of fact, MO-OOA shows wider potential source regions
598 than LO-OOA, which is assessed as fresh SOA and could be mainly formed at more local scale
599 in winter. Moreover, the impact of transport from northeastern regions – hosting intense
600 industrial activities - onto MO-OOA concentrations may also support a significant
601 anthropogenic origin for this SOA factor.

602 As shown in Figures 8c-d and S14, both MO-OOA and LO-OOA present high springtime
603 PSCF values originating from the northeastern regions too, which can participate in pollution
604 episodes frequently observed during this season (Petit et al., 2015; Srivastava et al., 2018b).
605 Therefore, mitigation of VOCs emissions at the regional scale could help to reduce the
606 substantial influence of OA on PM limit value exceedances during this season.

607 Narrower distribution of potential source regions was observed in summer and fall,
608 compared to winter and spring. MO-OOA presents potential source regions mainly from the
609 northeast in summer (Figure 8e), while it has a high potential source region originating from
610 the south in fall (Figure 8g). Finally, summertime LO-OOA, possibly from biogenic sources,
611 presented potential source regions from both northeast and south, suggesting the
612 contribution of a regional transport to the biogenic SOA production in summer.

613 All these results indicated that significant reduction of the SOA burden in the Paris
614 region does not only require the limitation of local source emissions, but also needs a
615 synergistic control strategy for the regional sources, especially from northeastern European
616 regions. In this respect, they confirmed conclusions reached by previous short-term
617 campaigns (e.g., Sciare et al., 2010; Crippa et al., 2013b; Freutel et al., 2013; Beekman et al.,
618 2015).

619

620 **5. Conclusions**

621 A comprehensive OA source apportionment has been achieved over the region of Paris from
622 November 2011 to March 2018. 4 factors, comprising HOA, BBOA, MO-OOA and LO-OOA, have
623 been identified and selected to ensure consistency of PMF factor solution over 6 years in this
624 study. Mean annual contributions of these factors to OA were of 11-16 % (HOA), 14-19%
625 (BBOA), 25-42 % (LO-OOA), and 30-45 % (MO-OOA), respectively. BBOA presented a



626 statistically significant seasonal pattern with highest concentrations during cold months, due
627 to residential wood burning emissions. The contribution of BBOA increased with increasing
628 concentration of OA mass in winter and fall – along with decreasing boundary layer height and
629 wind speed – highlighting the importance of biomass burning emissions for OA pollution under
630 stagnant meteorological conditions. HOA presented temporal variations similar to BBOA in
631 cold months, which was partly related to the fact that wood burning emissions also
632 contributed to HOA burden. BBOA and HOA exhibited very limited ($< 0.1 \mu\text{g m}^{-3} \text{yr}^{-1}$) or not
633 significant trends during the 6⁺-years investigated period. These results imply that specific
634 mitigation strategy, especially for residential wood burning, are still necessary for substantial
635 improvement of air quality in cold season in the Paris region.

636 LO-OOA and MO-OOA presented different seasonal variations, reflecting different
637 formation mechanisms and/or precursor sources. LO-OOA displayed a pronounced seasonal
638 cycle, with highest contribution total OA in summer (50-66 %) and lowest ones in winter (12-
639 19 %). Enhanced LO-OOA production during the warm season was assessed to be mainly
640 driven by biogenic SOA formation. This factor showed no significant long-term trend for the
641 studied period. MO-OOA presented higher contribution to OA at wintertime (35-51 %) and
642 springtime (32-62 %) than during the rest of the year. PSCF analyses suggested a high
643 probability of MO-OOA long-range transport from northeastern Europe towards the Paris
644 region. MO-OOA displayed a significant decreasing trend (of about $0.2 \mu\text{g m}^{-3} \text{yr}^{-1}$), which
645 might reflect the effect of emission control strategy of anthropogenic SOA precursors at the
646 regional scale over the last decade. However, future work is needed to fully understand
647 chemical properties of these SOA factors corresponding to different origins over different
648 seasons in the Paris region and to quantify the impact of emission control on ambient SOA
649 burden.

650

651 **Data availability.** The data have been presented in the text and figures as well as supplement.
652 Additional-related data will be available upon request.

653

654 **Competing interests.** The authors declare that they have no conflict of interest.

655



656 **Author contribution.** O.F., A.A., and V.G. designed and led the study. Y.Z. conducted the data analyses.
657 J-E.P., F.T., N.B., V.C., T.A., and J.S. provided the field observation. F. C. and A.P. supported the source
658 apportionment analyses. Y.Z. and O.F. interpreted the data, and wrote the manuscript, with inputs
659 from all coauthors.

660

661 **Acknowledgements.** This work has been part of the EU-FP7 and H2020 ACTRIS projects (grant
662 agreements no. 262254 and 654109) as well as the COLOSSAL COST action CA16109. It has also been
663 directly supported by the French Research Council (CNRS), the French alternatives energies and atomic
664 energy commission (CEA), and the French ministry of Environment through its funding to the reference
665 laboratory for air quality monitoring (LCSQA). Finally, Y. Zhang acknowledges the China Scholarship
666 Council (CSC) for PhD scholarship.

667



668 References

- 669 Aiken, A.C., DeCarlo, P.F., Kroll, J.H., Worsnop, D.R., Huffman, J.A., Docherty, K.S., Ulbrich, I.M., Mohr,
670 C., Kimmel, J.R., Sueper, D., Sun, Y., Zhang, Q., Trimborn, A., Northway, M., Ziemann, P.J.,
671 Canagaratna, M.R., Onasch, T.B., Alfarra, M.R., Prévôt, A.S.H., Dommen, J., Duplissy, J.,
672 Metzger, A., Baltensperger, U., and Jimenez, J.L.: O/C and OM/OC ratios of primary, secondary,
673 and ambient organic aerosols with high-resolution time-of-flight aerosol mass spectrometer,
674 *Environ. Sci. Technol.*, **42**, 4478–4485, 2008.
- 675 Alfarra, M. R., Prevot, A. S. H., Szidat, S., Sandradewi, J., Weimer, S., Lanz, V. A., Schreiber, D., Mohr,
676 M., and Baltensperger, U.: Identification of the Mass Spectral Signature of Organic Aerosols
677 from Wood Burning Emissions, *Environ. Sci. Technol.*, **41**, 5770-5777, 10.1021/es062289b,
678 2007.
- 679 Bae, M.-S., Demerjian, K. L., and Schwab, J. J.: Seasonal estimation of organic mass to organic carbon
680 in PM_{2.5} at rural and urban locations in New York state, *Atmos. Environ.*, **40**, 7467-7479,
681 <https://doi.org/10.1016/j.atmosenv.2006.07.008>, 2006.
- 682 Baudic, A., Gros, V., Sauvage, S., Locoge, N., Sanchez, O., Sarda-Estève, R., Kalogridis, C., Petit, J. E.,
683 Bonnaire, N., Baisnée, D., Favez, O., Albinet, A., Sciare, J., and Bonsang, B.: Seasonal variability
684 and source apportionment of volatile organic compounds (VOCs) in the Paris megacity (France),
685 *Atmos. Chem. Phys.*, **16**, 11961-11989, 10.5194/acp-16-11961-2016, 2016.
- 686 Beekmann, A. S. H. Prévôt, F. Drewnick, J. Sciare, S. N. Pandis, H. A. C. Denier van der Gon, M. Crippa,
687 F. Freutel, L. Poulain, V. Ghersi, E. Rodriguez, S. Beirle, P. Zotter, S.-L. von der Weiden-
688 Reinmüller, M. Bressi, C. Fountoukis, H. Petetin, S. Szidat, J. Schneider, A. Rosso, I. El Haddad,
689 A. Megaritis, Q.J. Zhang, V. Michoud, J.G. Slowik, S. Moukhtar, P. Kolmonen, A. Stohl, S.
690 Eckhardt, A. Borbon, V. Gros, N. Marchand, J.L. Jaffrezo, A. Schwarzenboeck, A. Colomb, A.
691 Wiedensohler, S. Borrmann, M. Lawrence, A. Baklanov, U. Baltensperger, In-situ, satellite
692 measurement and model evidence for a dominant regional contribution to fine particulate
693 matter levels in the Paris Megacity, *Atmos. Chem. Phys.*, **15**, 9577-9591, 2015.
- 694 Bertrand, A., Stefanelli, G., Bruns, E. A., Pieber, S. M., Temime-Roussel, B., Slowik, J. G., Prévôt, A. S. H.,
695 Wortham, H., El Haddad, I., and Marchand, N.: Primary emissions and secondary aerosol
696 production potential from woodstoves for residential heating: Influence of the stove
697 technology and combustion efficiency, *Atmos. Environ.*, **169**, 65-79,
698 <https://doi.org/10.1016/j.atmosenv.2017.09.005>, 2017.
- 699 Bressi, M., Sciare, J., Ghersi, V., Bonnaire, N., Nicolas, J. B., Petit, J.-E., Moukhtar, S., Rosso, A.,
700 Mihalopoulos, N., and Féron, A.: A one-year comprehensive chemical characterisation of fine
701 aerosol (PM_{2.5}) at urban, suburban and rural background sites in the region of Paris (France),
702 *Atmos. Chem. Phys.*, **13**, 7825-7844, <https://doi.org/10.5194/acp-13-7825-2013>, 2013.
- 703 Boucher, O., Randall, D., Artaxo, P., Bretherton, C., Feingold, G., Forster, P., Kerminen, V.-M., Kondo,
704 Y., Liao, H., Lohmann, U., Rasch, P., Satheesh, S. K., Sherwood, S., Stevens, B., and Zhang, X. Y.:
705 Clouds and Aerosols, in: *Climate Change 2013: The Physical Science Basis. Contribution of*
706 *Working Group I to the Fifth Assessment Report of the Intergovernmental Panel on Climate*
707 *Change*, edited by: Stocker, T. F., Qin, D., Plattner, G.-K., Tignor, M., Allen, S. K., Boschung, J.,
708 Nauels, A., Xia, Y., Bex, V., and Midgley, P. M., Cambridge University Press, Cambridge, United
709 Kingdom and New York, NY, USA, 571–658, 2013.
- 710 Bozzetti, C., El Haddad, I., Salameh, D., Daellenbach, K. R., Fermo, P., Gonzalez, R., Minguillón, M. C.,
711 Iinuma, Y., Poulain, L., Elser, M., Müller, E., Slowik, J. G., Jaffrezo, J. L., Baltensperger, U.,
712 Marchand, N., and Prévôt, A. S. H.: Organic aerosol source apportionment by offline-AMS over
713 a full year in Marseille, *Atmos. Chem. Phys.*, **17**, 8247-8268, 10.5194/acp-17-8247-2017, 2017.
- 714 Budisulistiorini, S. H., Li, X., Bairai, S. T., Renfro, J., Liu, Y., Liu, Y. J., McKinney, K. A., Martin, S. T., McNeill,
715 V. F., Pye, H. O. T., Nenes, A., Neff, M. E., Stone, E. A., Mueller, S., Knote, C., Shaw, S. L., Zhang,
716 Z., Gold, A. and Surratt, J. D.: Examining the effects of anthropogenic emissions on isoprene-
717 derived secondary organic aerosol formation during the 2013 Southern Oxidant and Aerosol
718 Study (SOAS) at the Look Rock, Tennessee ground site, *Atmos. Chem. Phys.*, **15**(15), 8871–8888,
719 doi:10.5194/acp-15-8871-2015, 2015.



- 720 Canagaratna, M. R., Jayne, J. T., Jimenez, J. L., Allan, J. D., Alfarra, M. R., Zhang, Q., Onasch, T. B.,
721 Drewnick, F., Coe, H., Middlebrook, A., Delia, A., Williams, L. R., Trimborn, A. M., Northway, M.
722 J., DeCarlo, P. F., Kolb, C. E., Davidovits, P., and Worsnop, D. R.: Chemical and microphysical
723 characterization of ambient aerosols with the aerodyne aerosol mass spectrometer, *Mass*
724 *Spectrom. Rev.*, 26, 185-222, 10.1002/mas.20115, 2007.
- 725 Canagaratna, M. R., Jimenez, J. L., Kroll, J.H., Chen, Q., Kessler, S.H., Massoli, P., Hildebrandt Ruiz, L.,
726 Fortner, E., Williams, L.R., Wilson, K.R., Surratt, J.D., Donahue, N.M., Jayne, J. T., and Worsnop,
727 D. R.: Elemental ratio measurements of organic compounds using aerosol mass spectrometry:
728 characterization, improved calibration, and implications, *Atmos. Chem. Phys.*, 15-253-272, doi:
729 10.5194/acp-15-253-2015, 2015.
- 730 Canonaco, F., Crippa, M., Slowik, J. G., Baltensperger, U., and Prévôt, A. S. H.: SoFi, an IGOR-based
731 interface for the efficient use of the generalized multilinear engine (ME-2) for the source
732 apportionment: ME-2 application to aerosol mass spectrometer data, *Atmos. Meas. Tech.*, 6,
733 3649-3661, 10.5194/amt-6-3649-2013, 2013.
- 734 Canonaco, F., Slowik, J. G., Baltensperger, U., and Prévôt, A. S. H.: Seasonal differences in oxygenated
735 organic aerosol composition: implications for emissions sources and factor analysis, *Atmos.*
736 *Chem. Phys.*, 15, 6993-7002, 10.5194/acp-15-6993-2015, 2015.
- 737 Cavalli, F., Viana, M., Yttri, K. E., Genberg, J., and Putaud, J. P.: Toward a standardised thermal-optical
738 protocol for measuring atmospheric organic and elemental carbon: the EUSAAR protocol,
739 *Atmos. Meas. Tech.*, 3, 79-89, 10.5194/amt-3-79-2010, 2010.
- 740 CITEPA, édition mars: Inventaire des émissions de polluants atmosphériques en France métropolitaine,
741 format CEE-NU, available at: [https://www.citepa.org/images/III-1_Rapports_Inventaires/CEE-](https://www.citepa.org/images/III-1_Rapports_Inventaires/CEE-NU/UNECE_France_mars2018.pdf)
742 [NU/UNECE_France_mars2018.pdf](https://www.citepa.org/images/III-1_Rapports_Inventaires/CEE-NU/UNECE_France_mars2018.pdf) (last access: May 2019), 2018.
- 743 Crenn, V., Sciare, J., Croteau, P. L., Verlhac, S., Fröhlich, R., Belis, C. A., Aas, W., Äijälä, M., Alastuey, A.,
744 Artiñano, B., Baisnée, D., Bonnaire, N., Bressi, M., Canagaratna, M., Canonaco, F., Carbone, C.,
745 Cavalli, F., Coz, E., Cubison, M. J., Esser-Gietl, J. K., Green, D. C., Gros, V., Heikkinen, L.,
746 Herrmann, H., Lunder, C., Minguillón, M. C., Močnik, G., O'Dowd, C. D., Ovadnevaite, J., Petit,
747 J. E., Petralia, E., Poulain, L., Priestman, M., Riffault, V., Ripoll, A., Sarda-Estève, R., Slowik, J. G.,
748 Setyan, A., Wiedensohler, A., Baltensperger, U., Prévôt, A. S. H., Jayne, J. T., and Favez, O.:
749 ACTRIS ACSM intercomparison – Part 1: Reproducibility of concentration and fragment results
750 from 13 individual Quadrupole Aerosol Chemical Speciation Monitors (Q-ACSM) and
751 consistency with co-located instruments, *Atmos. Meas. Tech.*, 8, 5063-5087, 10.5194/amt-8-
752 5063-2015, 2015.
- 753 Crippa, M., Canonaco, F., Slowik, J. G., El Haddad, I., DeCarlo, P. F., Mohr, C., Heringa, M. F., Chirico, R.,
754 Marchand, N., Temime-Roussel, B., Abidi, E., Poulain, L., Wiedensohler, A., Baltensperger, U.,
755 and Prévôt, A. S. H.: Primary and secondary organic aerosol origin by combined gas-particle
756 phase source apportionment, *Atmos. Chem. Phys.*, 13, 8411-8426, 10.5194/acp-13-8411-2013,
757 2013a.
- 758 Crippa, M., DeCarlo, P. F., Slowik, J. G., Mohr, C., Heringa, M. F., Chirico, R., Poulain, L., Freutel, F.,
759 Sciare, J., Cozic, J., Di Marco, C. F., Elsasser, M., Nicolas, J. B., Marchand, N., Abidi, E.,
760 Wiedensohler, A., Drewnick, F., Schneider, J., Borrmann, S., Nemitz, E., Zimmermann, R.,
761 Jaffrezou, J. L., Prévôt, A. S. H., and Baltensperger, U.: Wintertime aerosol chemical composition
762 and source apportionment of the organic fraction in the metropolitan area of Paris, *Atmos.*
763 *Chem. Phys.*, 13, 961-981, 10.5194/acp-13-961-2013, 2013b.
- 764 Crippa, M., El Haddad, I., Slowik, J. G., DeCarlo, P. F., Mohr, C., Heringa, M. F., Chirico, R., Marchand,
765 N., Sciare, J., Baltensperger, U., and Prévôt, A. S. H.: Identification of marine and continental
766 aerosol sources in Paris using high resolution aerosol mass spectrometry, *J. Geophys. Res.*
767 *Atmos.*, 118, 1950-1963, doi:10.1002/jgrd.50151, 2013c.
- 768 Crippa, M., Canonaco, F., Lanz, V. A., Äijälä, M., Allan, J. D., Carbone, S., Capes, G., Ceburnis, D.,
769 Dall'Osto, M., Day, D. A., DeCarlo, P. F., Ehn, M., Eriksson, A., Freney, E., Hildebrandt Ruiz, L.,
770 Hillamo, R., Jimenez, J. L., Junninen, H., Kiendler-Scharr, A., Kortelainen, A. M., Kulmala, M.,
771 Laaksonen, A., Mensah, A. A., Mohr, C., Nemitz, E., O'Dowd, C., Ovadnevaite, J., Pandis, S. N.,



- 772 Petäjä, T., Poulain, L., Saarikoski, S., Sellegri, K., Swietlicki, E., Tiitta, P., Worsnop, D. R.,
773 Baltensperger, U., and Prévôt, A. S. H.: Organic aerosol components derived from 25 AMS data
774 sets across Europe using a consistent ME-2 based source apportionment approach, *Atmos.*
775 *Chem. Phys.*, 14, 6159-6176, 10.5194/acp-14-6159-2014, 2014.
- 776 Daellenbach, K. R., Kourtchev, I., Vogel, A. L., Bruns, E. A., Jiang, J., Petäjä, T., Jaffrezo, J. L., Aksoyoglu,
777 S., Kalberer, M., Baltensperger, U., El Haddad, I., and Prévôt, A. S. H.: Impact of anthropogenic
778 and biogenic sources on the seasonal variation in the molecular composition of urban organic
779 aerosols: a field and laboratory study using ultra-high-resolution mass spectrometry, *Atmos.*
780 *Chem. Phys.*, 19, 5973-5991, 10.5194/acp-19-5973-2019, 2019.
- 781 Daellenbach, K. R., Stefenelli, G., Bozzetti, C., Vlachou, A., Fermo, P., Gonzalez, R., Piazzalunga, A.,
782 Colombi, C., Canonaco, F., Hueglin, C., Kasper-Giebl, A., Jaffrezo, J. L., Bianchi, F., Slowik, J. G.,
783 Baltensperger, U., El-Haddad, I., and Prévôt, A. S. H.: Long-term chemical analysis and organic
784 aerosol source apportionment at nine sites in central Europe: source identification and
785 uncertainty assessment, *Atmos. Chem. Phys.*, 17, 13265-13282, 10.5194/acp-17-13265-2017,
786 2017.
- 787 Dall'Osto, M., Paglione, M., Decesari, S., Facchini, M. C., O'Dowd, C., Plass-Duellmer, C., and Harrison,
788 R. M.: On the Origin of AMS "Cooking Organic Aerosol" at a Rural Site, *Environ. Sci. Technol.*,
789 49, 13964-13972, 10.1021/acs.est.5b02922, 2015.
- 790 Draxler, R. R., and Rolph, G.D.: HYSPLIT (HYbrid Single-Particle Lagrangian Integrated Trajectory) Model
791 Access via NOAA ARL READY Website. NOAA Air Resources Laboratory, Silver Spring, MD.
792 <http://www.arl.noaa.gov/ready/hysplit4.html>, 2003.
- 793 Drinovec, L., Močnik, G., Zotter, P., Prévôt, A. S. H., Ruckstuhl, C., Coz, E., Rupakheti, M., Sciare, J.,
794 Müller, T., Wiedensohler, A., and Hansen, A. D. A.: The "dual-spot" Aethalometer: an improved
795 measurement of aerosol black carbon with real-time loading compensation, *Atmos. Meas.*
796 *Tech.*, 8, 1965-1979, 10.5194/amt-8-1965-2015, 2015.
- 797 Drinovec, L., Gregorič, A., Zotter, P., Wolf, R., Bruns, E. A., Prévôt, A. S. H., Petit, J. E., Favez, O., Sciare,
798 J., Arnold, I. J., Chakrabarty, R. K., Moosmüller, H., Filep, A., and Močnik, G.: The filter-loading
799 effect by ambient aerosols in filter absorption photometers depends on the coating of the
800 sampled particles, *Atmos. Meas. Tech.*, 10, 1043-1059, 10.5194/amt-10-1043-2017, 2017.
- 801 Dupont, J.-C., Haefelin, M., Badosa, J., Elias, T., Favez, O., Petit, J.-E., Meleux, F., Sciare, J., Crenn, V.,
802 and Bonne, J.-L.: Role of the boundary layer dynamics effects on an extreme air pollution event
803 in Paris, *Atmos. Environ.*, 141, 571-579, doi: 10.1016/j.atmosenv.2016.06.061, 2016.
- 804 EMEP: Air pollution trends in the EMEP region between 1990 and 2012. CCC-report 1/2016, available
805 at [http://publications.iass-](http://publications.iass-potsdam.de/pubman/item/escidoc:1622889:8/component/escidoc:1622890/1622889.pdf)
806 [potsdam.de/pubman/item/escidoc:1622889:8/component/escidoc:1622890/1622889.pdf](http://publications.iass-potsdam.de/pubman/item/escidoc:1622889:8/component/escidoc:1622890/1622889.pdf)
807 (last access: May 2019), 2016
- 808 Favez, O., Cachier, H., Sciare, J., Sarda-Estève, R., and Martinon, L.: Evidence for a significant
809 contribution of wood burning aerosols to PM_{2.5} during the winter season in Paris, France,
810 *Atmos. Environ.*, 43, 3640-3644, <https://doi.org/10.1016/j.atmosenv.2009.04.035>, 2009.
- 811 Favez, O., El Haddad, I., Piot, C., Boréave, A., Abidi, E., Marchand, N., Jaffrezo, J.L., Besombes, J.L.,
812 Personnaz, M.B., Sciare, J., Wortham, H., George, C., and D'Anna, B.: Inter-comparison of
813 source apportionment models for the estimation of wood burning aerosols during wintertime
814 in an Alpine city (Grenoble, France), *Atmos. Chem. Phys.*, 10, 5295-5314, 2010.
- 815 Freney, E., Sellegri, K., Chrit, M., Adachi, K., Brito, J., Waked, A., Borbon, A., Colomb, A., Dupuy, R.,
816 Pichon, J. M., Bouvier, L., Delon, C., Jambert, C., Durand, P., Bourianne, T., Gaimoz, C., Triquet,
817 S., Féron, A., Beekmann, M., Dulac, F., and Sartelet, K.: Aerosol composition and the
818 contribution of SOA formation over Mediterranean forests, *Atmos. Chem. Phys.*, 18, 7041-
819 7056, 10.5194/acp-18-7041-2018, 2018.
- 820 Freney, E., Zhang, Y., Croteau, P., Amodeo, T., Williams, L., Truong, F., Petit, J.-E., Sciare, J., Sarda-Estève,
821 R., Bonnaire, N., Arumae, T., Aurela, M., Bougiatioti, A., Mihalopoulos, N., Coz, E., Artinano, B.,
822 Crenn, V., Elste, T., Heikkinen, L., Poulain, L., Wiedensohler, A., Herrmann, H., Priestman, M.,
823 Alastuey, A., Stavroulas, I., Tobler, A., Vasilescu, J., Zanca, N., Canagaratna, M., Carbone, C.,



- 824 Flentje, H., Green, D., Maasikmets, M., Marmureanu, L., Minguillon, M. C., Prevot, A. S. H.,
825 Gros, V., Jayne, J., and Favez, O.: The second ACTRIS inter-comparison (2016) for Aerosol
826 Chemical Speciation Monitors (ACSM): Calibration protocols and instrument performance
827 evaluations, *Aerosol Sci. Technol.*, 1-25, 10.1080/02786826.2019.1608901, 2019.
- 828 Freutel, F., Schneider, J., Drewnick, F., von der Weiden-Reinmüller, S. L., Crippa, M., Prévôt, A. S. H.,
829 Baltensperger, U., Poulain, L., Wiedensohler, A., Sciare, J., Sarda-Estève, R., Burkhardt, J. F.,
830 Eckhardt, S., Stohl, A., Gros, V., Colomb, A., Michoud, V., Doussin, J. F., Borbon, A., Haeffelin,
831 M., Morille, Y., Beekmann, M., and Borrmann, S.: Aerosol particle measurements at three
832 stationary sites in the megacity of Paris during summer 2009: meteorology and air mass origin
833 dominate aerosol particle composition and size distribution, *Atmos. Chem. Phys.*, 13, 933-959,
834 10.5194/acp-13-933-2013, 2013.
- 835 Fröhlich, R., Crenn, V., Setyan, A., Belis, C. A., Canonaco, F., Favez, O., Riffault, V., Slowik, J. G., Aas, W.,
836 Aijälä, M., Alastuey, A., Artiñano, B., Bonnaire, N., Bozzetti, C., Bressi, M., Carbone, C., Coz, E.,
837 Croteau, P. L., Cubison, M. J., Esser-Gietl, J. K., Green, D. C., Gros, V., Heikkinen, L., Herrmann,
838 H., Jayne, J. T., Lunder, C. R., Minguillón, M. C., Močnik, G., O'Dowd, C. D., Ovadnevaite, J.,
839 Petralia, E., Poulain, L., Priestman, M., Ripoll, A., Sarda-Estève, R., Wiedensohler, A.,
840 Baltensperger, U., Sciare, J., and Prévôt, A. S. H.: ACTRIS ACSM intercomparison – Part 2:
841 Intercomparison of ME-2 organic source apportionment results from 15 individual, co-located
842 aerosol mass spectrometers, *Atmos. Meas. Tech.*, 8, 2555-2576, 10.5194/amt-8-2555-2015,
843 2015b.
- 844 Fröhlich, R., Cubison, M. J., Slowik, J. G., Bukowiecki, N., Canonaco, F., Croteau, P. L., Gysel, M., Henne,
845 S., Herrmann, E., Jayne, J. T., Steinbacher, M., Worsnop, D. R., Baltensperger, U., and Prévôt,
846 A. S. H.: Fourteen months of on-line measurements of the non-refractory submicron aerosol
847 at the Jungfraujoch (3580 m a.s.l.) – chemical composition, origins and organic aerosol sources,
848 *Atmos. Chem. Phys.*, 15, 11373-11398, <https://doi.org/10.5194/acp-15-11373-2015>, 2015a.
- 849 Gentner, D. R., Jathar, S. H., Gordon, T. D., Bahreini, R., Day, D. A., El Haddad, I., Hayes, P. L., Pieber, S.
850 M., Platt, S. M., de Gouw, J., Goldstein, A. H., Harley, R. A., Jimenez, J. L., Prévôt, A. S. H., and
851 Robinson, A. L.: Review of Urban Secondary Organic Aerosol Formation from Gasoline and
852 Diesel Motor Vehicle Emissions, *Environ. Sci. Technol.*, 51, 1074-1093,
853 10.1021/acs.est.6b04509, 2017.
- 854 Gilardoni, S., Massoli, P., Paglione, M., Giulianelli, L., Carbone, C., Rinaldi, M., Decesari, S., Sandrini, S.,
855 Costabile, F., Gobbi, G. P., Pietrogrande, M. C., Visentin, M., Scotto, F., Fuzzi, S., and Facchini,
856 M. C.: Direct observation of aqueous secondary organic aerosol from biomass-burning
857 emissions, *Proc. Natl. Acad. Sci. U. S. A.*, 113, 10013-10018, 10.1073/pnas.1602212113, 2016.
- 858 Goldstein, A. H., Koven, C. D., Heald, C. L., and Fung, I. Y.: Biogenic carbon and anthropogenic pollutants
859 combine to form a cooling haze over the southeastern United States, *Proc. Natl. Acad. Sci. U.*
860 *S. A.*, 106, 8835-8840, 10.1073/pnas.0904128106, 2009.
- 861 Grieshop, A. P., Donahue, N. M., and Robinson, A. L.: Laboratory investigation of photochemical
862 oxidation of organic aerosol from wood fires 2: analysis of aerosol mass spectrometer data,
863 *Atmos. Chem. Phys.*, 9, 2227-2240, <https://doi.org/10.5194/acp-9-2227-2009>, 2009.
- 864 Haeffelin, M., Barthès, L., Bock, O., Boitel, C., Bony, S., Bouniol, D., Chepfer, H., Chiriaco, M., Cuesta, J.,
865 Delanoë, J., Drobinski, P., Dufresne, J. L., Flamant, C., Grall, M., Hodzic, A., Hourdin, F., Lapouge,
866 F., Lemaître, Y., Mathieu, A., Morille, Y., Naud, C., Noël, V., O'Hirok, W., Pelon, J., Pietras, C.,
867 Protat, A., Romand, B., Scialom, G., and Vautard, R.: SIRTa, a ground-based atmospheric
868 observatory for cloud and aerosol research, *Ann. Geophys.*, 23, 253-275, 10.5194/angeo-23-
869 253-2005, 2005.
- 870 Hallquist, M., Wenger, J. C., Baltensperger, U., Rudich, Y., Simpson, D., Claeys, M., Dommen, J.,
871 Donahue, N. M., George, C., Goldstein, A. H., Hamilton, J. F., Herrmann, H., Hoffmann, T.,
872 Iinuma, Y., Jang, M., Jenkin, M. E., Jimenez, J. L., Kiendler-Scharr, A., Maenhaut, W., McFiggans,
873 G., Mentel, T. F., Monod, A., Prévôt, A. S. H., Seinfeld, J. H., Surratt, J. D., Szmigielski, R., and
874 Wildt, J.: The formation, properties and impact of secondary organic aerosol: current and
875 emerging issues, *Atmos. Chem. Phys.*, 9, 5155-5236, 10.5194/acp-9-5155-2009, 2009.



- 876 Heringa, M. F., DeCarlo, P. F., Chirico, R., Tritscher, T., Dommen, J., Weingartner, E., Richter, R., Wehrle,
877 G., Prévôt, A. S. H., and Baltensperger, U.: Investigations of primary and secondary particulate
878 matter of different wood combustion appliances with a high-resolution time-of-flight aerosol
879 mass spectrometer, *Atmos. Chem. Phys.*, 11, 5945-5957, 10.5194/acp-11-5945-2011, 2011.
- 880 Jayne, J. T., Leard, D. C., Zhang, X., Davidovits, P., Smith, K. A., Kolb, C. E., and Worsnop, D. R.:
881 Development of an Aerosol Mass Spectrometer for Size and Composition Analysis of
882 Submicron Particles, *Aerosol Sci. Technol.*, 33, 49-70, 10.1080/027868200410840, 2000.
- 883 Jimenez, J. L., Canagaratna, M. R., Donahue, N. M., Prevot, A. S. H., Zhang, Q., Kroll, J. H., DeCarlo, P.
884 F., Allan, J. D., Coe, H., Ng, N. L., Aiken, A. C., Docherty, K. S., Ulbrich, I. M., Grieshop, A. P.,
885 Robinson, A. L., Duplissy, J., Smith, J. D., Wilson, K. R., Lanz, V. A., Hueglin, C., Sun, Y. L., Tian,
886 J., Laaksonen, A., Raatikainen, T., Rautiainen, J., Vaattovaara, P., Ehn, M., Kulmala, M.,
887 Tomlinson, J. M., Collins, D. R., Cubison, M. J., Dunlea, J., Huffman, J. A., Onasch, T. B., Alfarra,
888 M. R., Williams, P. I., Bower, K., Kondo, Y., Schneider, J., Drewnick, F., Borrmann, S., Weimer,
889 S., Demerjian, K., Salcedo, D., Cottrell, L., Griffin, R., Takami, A., Miyoshi, T., Hatakeyama, S.,
890 Shimono, A., Sun, J. Y., Zhang, Y. M., Dzepina, K., Kimmel, J. R., Sueper, D., Jayne, J. T., Herndon,
891 S. C., Trimborn, A. M., Williams, L. R., Wood, E. C., Middlebrook, A. M., Kolb, C. E.,
892 Baltensperger, U., and Worsnop, D. R.: Evolution of Organic Aerosols in the Atmosphere,
893 *Science*, 326, 1525-1529, 10.1126/science.1180353, 2009.
- 894 Kroll, J. H., and Seinfeld, J. H.: Chemistry of secondary organic aerosol: Formation and evolution of low-
895 volatility organics in the atmosphere, *Atmos. Environ.*, 42, 3593-3624,
896 10.1016/j.atmosenv.2008.01.003, 2008.
- 897 Kruskal, W. H., and Wallis, W. A.: Use of Ranks in One-Criterion Variance Analysis, *J. Am. Stat. Assoc.*,
898 47, 583-621, 10.2307/2280779, 1952.
- 899 Lanz, V. A., Alfarra, M. R., Baltensperger, U., Buchmann, B., Hueglin, C., and Prévôt, A. S. H.: Source
900 apportionment of submicron organic aerosols at an urban site by factor analytical modelling
901 of aerosol mass spectra, *Atmos. Chem. Phys.*, 7, 1503-1522, 10.5194/acp-7-1503-2007, 2007.
- 902 Lanz, V. A., Prévôt, A. S. H., Alfarra, M. R., Weimer, S., Mohr, C., DeCarlo, P. F., Gianini, M. F. D., Hueglin,
903 C., Schneider, J., Favez, O., D'Anna, B., George, C., and Baltensperger, U.: Characterization of
904 aerosol chemical composition with aerosol mass spectrometry in Central Europe: an overview,
905 *Atmos. Chem. Phys.*, 10, 10453-10471, 10.5194/acp-10-10453-2010, 2010.
- 906 Leaitch, W. R., Macdonald, A. M., Brickell, P. C., Liggio, J., Sjostedt, S. J., Vlasenko, A., Bottenheim, J.
907 W., Huang, L., Li, S.-M., Liu, P. S. K., Toom-Sauntry, D., Hayden, K. A., Sharma, S., Shantz, N. C.,
908 Wiebe, H. A., Zhang, W., Abbatt, J. P. D., Slowik, J. G., Chang, R. Y. W., Russell, L. M., Schwartz,
909 R. E., Takahama, S., Jayne, J. T., and Ng, N. L.: Temperature response of the submicron organic
910 aerosol from temperate forests, *Atmos. Environ.*, 45, 6696-6704,
911 <https://doi.org/10.1016/j.atmosenv.2011.08.047>, 2011.
- 912 Li, Y. J., Sun, Y., Zhang, Q., Li, X., Li, M., Zhou, Z., and Chan, C. K.: Real-time chemical characterization
913 of atmospheric particulate matter in China: A review, *Atmos. Environ.*, 158, 270-304,
914 <https://doi.org/10.1016/j.atmosenv.2017.02.027>, 2017.
- 915 Liu, P. S. K., Deng, R., Smith, K. A., Williams, L. R., Jayne, J. T., Canagaratna, M. R., Moore, K., Onasch,
916 T. B., Worsnop, D. R., and Deshler, T.: Transmission Efficiency of an Aerodynamic Focusing Lens
917 System: Comparison of Model Calculations and Laboratory Measurements for the Aerodyne
918 Aerosol Mass Spectrometer, *Aerosol Sci. Technol.*, 41, 721-733, 10.1080/02786820701422278,
919 2007.
- 920 Mann, H. B.: Nonparametric Tests Against Trend, *Econometrica*, 13, 245-259, 10.2307/1907187, 1945.
- 921 Ng, N. L., Canagaratna, M. R., Zhang, Q., Jimenez, J. L., Tian, J., Ulbrich, I. M., Kroll, J. H., Docherty, K.
922 S., Chhabra, P. S., Bahreini, R., Murphy, S. M., Seinfeld, J. H., Hildebrandt, L., Donahue, N. M.,
923 DeCarlo, P. F., Lanz, V. A., Prévôt, A. S. H., Dinar, E., Rudich, Y., and Worsnop, D. R.: Organic
924 aerosol components observed in Northern Hemispheric datasets from Aerosol Mass
925 Spectrometry, *Atmos. Chem. Phys.*, 10, 4625-4641, 10.5194/acp-10-4625-2010, 2010.



- 926 Ng, N. L., Canagaratna, M. R., Jimenez, J. L., Chhabra, P. S., Seinfeld, J. H., and Worsnop, D. R.: Changes
927 in organic aerosol composition with aging inferred from aerosol mass spectra, *Atmos. Chem.*
928 *Phys.*, 11, 6465-6474, 10.5194/acp-11-6465-2011, 2011a.
- 929 Ng, N. L., Herndon, S. C., Trimborn, A., Canagaratna, M. R., Croteau, P. L., Onasch, T. B., Sueper, D.,
930 Worsnop, D. R., Zhang, Q., Sun, Y. L., and Jayne, J. T.: An Aerosol Chemical Speciation Monitor
931 (ACSM) for Routine Monitoring of the Composition and Mass Concentrations of Ambient
932 Aerosol, *Aerosol Sci. Technol.*, 45, 780-794, 10.1080/02786826.2011.560211, 2011b.
- 933 Nozière, B., Kalberer, M., Claeys, M., Allan, J., D'Anna, B., Decesari, S., Finessi, E., Glasius, M., Grgić, I.,
934 Hamilton, J. F., Hoffmann, T., Iinuma, Y., Jaoui, M., Kahnt, A., Kampf, C. J., Kourtchev, I.,
935 Maenhaut, W., Marsden, N., Saarikoski, S., Schnelle-Kreis, J., Surratt, J. D., Szidat, S., Szmigielski,
936 R., and Wisthaler, A.: The Molecular Identification of Organic Compounds in the Atmosphere:
937 State of the Art and Challenges, *Chem. Rev.*, 115, 3919-3983, 10.1021/cr5003485, 2015.
- 938 Paatero, P., and Tapper, U.: Positive matrix factorization: A non-negative factor model with optimal
939 utilization of error estimates of data values, *Environmetrics*, 5, 111-126,
940 doi:10.1002/env.3170050203, 1994.
- 941 Paatero, P.: The Multilinear Engine—A Table-Driven, Least Squares Program for Solving Multilinear
942 Problems, Including the n-Way Parallel Factor Analysis Model, *J. Comput. Graph. Stat.*, 8, 854-
943 888, 10.1080/10618600.1999.10474853, 1999.
- 944 Pandolfi, M., Alados-Arboledas, L., Alastuey, A., Andrade, M., Angelov, C., Artiñano, B., Backman, J.,
945 Baltensperger, U., Bonasoni, P., Bukowiecki, N., Collaud Coen, M., Conil, S., Coz, E., Crenn, V.,
946 Dudoitis, V., Ealo, M., Eleftheriadis, K., Favez, O., Fetfatzis, P., Fiebig, M., Flentje, H., Ginot, P.,
947 Gysel, M., Henzing, B., Hoffer, A., Holubova Smejkalova, A., Kalapov, I., Kalivitis, N., Kouvarakis,
948 G., Kristensson, A., Kulmala, M., Lihavainen, H., Lunder, C., Luoma, K., Lyamani, H., Marinoni,
949 A., Mihalopoulos, N., Moerman, M., Nicolas, J., O'Dowd, C., Petäjä, T., Petit, J. E., Pichon, J. M.,
950 Prokopciuk, N., Putaud, J. P., Rodríguez, S., Sciare, J., Sellegri, K., Swietlicki, E., Titos, G., Tuch,
951 T., Tunved, P., Ulevicius, V., Vaishya, A., Vana, M., Virkkula, A., Vratolis, S., Weingartner, E.,
952 Wiedensohler, A., and Laj, P.: A European aerosol phenomenology – 6: scattering properties
953 of atmospheric aerosol particles from 28 ACTRIS sites, *Atmos. Chem. Phys.*, 18, 7877-7911,
954 10.5194/acp-18-7877-2018, 2018.
- 955 Petit, J. E., Favez, O., Sciare, J., Canonaco, F., Croteau, P., Močnik, G., Jayne, J., Worsnop, D., and Leoz-
956 Garziandia, E.: Submicron aerosol source apportionment of wintertime pollution in Paris,
957 France by double positive matrix factorization (PMF²) using an aerosol chemical
958 speciation monitor (ACSM) and a multi-wavelength Aethalometer, *Atmos. Chem. Phys.*, 14,
959 13773-13787, 10.5194/acp-14-13773-2014, 2014.
- 960 Petit, J. E., Favez, O., Sciare, J., Crenn, V., Sarda-Estève, R., Bonnaire, N., Močnik, G., Dupont, J. C.,
961 Haefelin, M., and Leoz-Garziandia, E.: Two years of near real-time chemical composition of
962 submicron aerosols in the region of Paris using an Aerosol Chemical Speciation Monitor (ACSM)
963 and a multi-wavelength Aethalometer, *Atmos. Chem. Phys.*, 15, 2985-3005, 10.5194/acp-15-
964 2985-2015, 2015.
- 965 Petit, J. E., Favez, O., Albinet, A., and Canonaco, F.: A user-friendly tool for comprehensive evaluation
966 of the geographical origins of atmospheric pollution: Wind and trajectory analyses, *Environ.*
967 *Modell. Softw.*, 88, 183-187, <http://dx.doi.org/10.1016/j.envsoft.2016.11.022>, 2017.
- 968 Pohlert, T.: Package 'trend', 2018.
- 969 Polissar, A. V., Hopke, P. K., Paatero, P., Kaufmann, Y. J., Hall, D. K., Bodhaine, B. A., Dutton, E. G., and
970 Harris, J. M.: The aerosol at Barrow, Alaska: long-term trends and source locations, *Atmos.*
971 *Environ.*, 33, 2441-2458, [https://doi.org/10.1016/S1352-2310\(98\)00423-3](https://doi.org/10.1016/S1352-2310(98)00423-3), 1999.
- 972 Rattanavaraha, W., Canagaratna, M. R., Budisulistiorini, S. H., Croteau, P. L., Baumann, K., Canonaco,
973 F., Prevot, A. S. H., Edgerton, E. S., Zhang, Z., Jayne, J. T., Worsnop, D. R., Gold, A., Shaw, S. L.,
974 and Surratt, J. D.: Source apportionment of submicron organic aerosol collected from Atlanta,
975 Georgia, during 2014–2015 using the aerosol chemical speciation monitor (ACSM), *Atmos.*
976 *Environ.*, 167, 389–402, 2017.



- 977 Reyes-Villegas, E., Green, D. C., Priestman, M., Canonaco, F., Coe, H., Prévôt, A. S. H., and Allan, J. D.:
978 Organic aerosol source apportionment in London 2013 with ME-2: exploring the solution space
979 with annual and seasonal analysis, *Atmos. Chem. Phys.*, 16, 15545-15559, 10.5194/acp-16-
980 15545-2016, 2016.
- 981 Sandradewi, J., Prévôt, A. S. H., Szidat, S., Perron, N., Alfarra, M. R., Lanz, V. A., Weingartner, E., and
982 Baltensperger, U.: Using Aerosol Light Absorption Measurements for the Quantitative
983 Determination of Wood Burning and Traffic Emission Contributions to Particulate Matter,
984 *Environ. Sci. Technol.*, 42, 3316-3323, 10.1021/es702253m, 2008.
- 985 Schlag, P., Kiendler-Scharr, A., Blom, M. J., Canonaco, F., Henzing, J. S., Moerman, M., Prévôt, A. S. H.,
986 and Holzinger, R.: Aerosol source apportionment from 1-year measurements at the CESAR
987 tower in Cabauw, the Netherlands, *Atmos. Chem. Phys.*, 16, 8831-8847, 10.5194/acp-16-8831-
988 2016, 2016.
- 989 Schurgers, G., Arneth, A., Holzinger, R., and Goldstein, A. H.: Process-based modelling of biogenic
990 monoterpene emissions combining production and release from storage, *Atmos. Chem. Phys.*,
991 9, 3409-3423, 10.5194/acp-9-3409-2009, 2009.
- 992 Sciare, J., d'Argouges, O., Zhang, Q. J., Sarda-Estève, R., Gaimoz, C., Gros, V., Beekmann, M., and
993 Sanchez, O.: Comparison between simulated and observed chemical composition of fine
994 aerosols in Paris (France) during springtime: contribution of regional versus continental
995 emissions, *Atmos. Chem. Phys.*, 10, 11987-12004, 10.5194/acp-10-11987-2010, 2010.
- 996 Sciare, J., d'Argouges, O., Sarda-Estève, R., Gaimoz, C., Dolgorouky, C., Bonnaire, N., Favez, O., Bonsang,
997 B., and Gros, V.: Large contribution of water-insoluble secondary organic aerosols in the region
998 of Paris (France) during wintertime, *J. Geophys. Res. Atmos.*, 116, doi:10.1029/2011JD015756,
999 2011.
- 1000 Sen, P. K.: Estimates of the Regression Coefficient Based on Kendall's Tau, *J. Am. Stat. Assoc.*, 63, 1379-
1001 1389, 10.2307/2285891, 1968.
- 1002 Shapiro, S. S., and Wilk, M. B.: An Analysis of Variance Test for Normality (Complete Samples),
1003 *Biometrika*, 52, 591-611, 10.2307/2333709, 1965.
- 1004 Shrivastava, M., Cappa, C. D., Fan, J., Goldstein, A. H., Guenther, A. B., Jimenez, J. L., Kuang, C., Laskin,
1005 A., Martin, S. T., Ng, N. L., Petaja, T., Pierce, J. R., Rasch, P. J., Roldin, P., Seinfeld, J. H., Shilling,
1006 J., Smith, J. N., Thornton, J. A., Volkamer, R., Wang, J., Worsnop, D. R., Zaveri, R. A., Zelenyuk,
1007 A., and Zhang, Q.: Recent advances in understanding secondary organic aerosol: Implications
1008 for global climate forcing, *Reviews of Geophysics*, 55, 509-559, doi:10.1002/2016RG000540,
1009 2017.
- 1010 Srivastava, D., Favez, O., Perraudin, E., Villenave, E., and Albinet, A.: Comparison of Measurement-
1011 Based Methodologies to Apportion Secondary Organic Carbon (SOC) in PM_{2.5}: A Review of
1012 Recent Studies, *Atmosphere*, 9, 452, 2018a.
- 1013 Srivastava, D., Favez, O., Bonnaire, N., Lucarelli, F., Haeffelin, M., Perraudin, E., Gros, V., Villenave, E.,
1014 and Albinet, A.: Speciation of organic fractions does matter for aerosol source apportionment.
1015 Part 2: Intensive short-term campaign in the Paris area (France), *Sci. Total Environ.*, 634, 267-
1016 278, <https://doi.org/10.1016/j.scitotenv.2018.03.296>, 2018b.
- 1017 Srivastava, D., Daellenbach, K.R., Zhang, Y., Bonnaire, N., Chazeanu, B., Perraudin, E., Gros, V., Villenave,
1018 E., Prévôt, A.S.H., El Haddad, I., Favez, O., and Albinet, A.: Comparison of different
1019 methodologies to discriminate between primary and secondary organic aerosols, *Sci. Total
1020 Environ.*, accepted for publication.
- 1021 Stein, A.F., Draxler, R.R., Rolph, G.D., Stunder, B.J.B., Cohen, M.D., Ngan, F.: NOAA's HYSPLIT
1022 atmospheric transport and dispersion modeling System. *Bull. Am. Meteorol. Soc.* 96 (12),
1023 2059e2077. <http://dx.doi.org/10.1175/BAMS-D-14-00110.1>, 2015.
- 1024 Sun, Y. L., Zhang, Q., Schwab, J. J., Demerjian, K. L., Chen, W. N., Bae, M. S., Hung, H. M., Hogrefe, O.,
1025 Frank, B., Rattigan, O. V., and Lin, Y. C.: Characterization of the sources and processes of
1026 organic and inorganic aerosols in New York city with a high-resolution time-of-flight aerosol
1027 mass spectrometer, *Atmos. Chem. Phys.*, 11, 1581-1602, 10.5194/acp-11-1581-2011, 2011.



- 1028 Sun, Y., Wang, Z., Dong, H., Yang, T., Li, J., Pan, X., Chen, P., and Jayne, J. T.: Characterization of summer
1029 organic and inorganic aerosols in Beijing, China with an Aerosol Chemical Speciation Monitor,
1030 *Atmos. Environ.*, **51**, 250-259, <https://doi.org/10.1016/j.atmosenv.2012.01.013>, 2012.
- 1031 Sun, Y., Xu, W., Zhang, Q., Jiang, Q., Canonaco, F., Prévôt, A. S. H., Fu, P., Li, J., Jayne, J., Worsnop, D. R.,
1032 and Wang, Z.: Source apportionment of organic aerosol from 2-year highly time-resolved
1033 measurements by an aerosol chemical speciation monitor in Beijing, China, *Atmos. Chem.
1034 Phys.*, **18**, 8469-8489, [10.5194/acp-18-8469-2018](https://doi.org/10.5194/acp-18-8469-2018), 2018.
- 1035 Tiitta, P., Leskinen, A., Hao, L., Yli-Pirilä, P., Kortelainen, M., Grigonyte, J., Tissari, J., Lamberg, H.,
1036 Hartikainen, A., Kuusalo, K., Kortelainen, A. M., Virtanen, A., Lehtinen, K. E. J., Komppula, M.,
1037 Pieber, S., Prévôt, A. S. H., Onasch, T. B., Worsnop, D. R., Czech, H., Zimmermann, R., Jokiniemi,
1038 J., and Sippula, O.: Transformation of logwood combustion emissions in a smog chamber:
1039 formation of secondary organic aerosol and changes in the primary organic aerosol upon
1040 daytime and nighttime aging, *Atmos. Chem. Phys.*, **16**, 13251-13269, [10.5194/acp-16-13251-
1041 2016](https://doi.org/10.5194/acp-16-13251-2016), 2016.
- 1042 Ulbrich, I. M., Canagaratna, M. R., Zhang, Q., Worsnop, D. R., and Jimenez, J. L.: Interpretation of
1043 organic components from Positive Matrix Factorization of aerosol mass spectrometric data,
1044 *Atmos. Chem. Phys.*, **9**, 2891-2918, [10.5194/acp-9-2891-2009](https://doi.org/10.5194/acp-9-2891-2009), 2009.
- 1045 Waked, A., Favez, O., Alleman, L. Y., Piot, C., Petit, J. E., Delaunay, T., Verlinden, E., Golly, B., Besombes,
1046 J. L., Jaffrezo, J. L., and Leoz-Garziandia, E.: Source apportionment of PM₁₀ in a
1047 north-western Europe regional urban background site (Lens, France) using positive matrix
1048 factorization and including primary biogenic emissions, *Atmos. Chem. Phys.*, **14**, 3325-3346,
1049 [10.5194/acp-14-3325-2014](https://doi.org/10.5194/acp-14-3325-2014), 2014.
- 1050 Xu, L., Guo, H., Boyd, C. M., Klein, M., Bougiatioti, A., Cerully, K. M., Hite, J. R., Isaacman-VanWertz, G.,
1051 Kreisberg, N. M., Knote, C., Olson, K., Koss, A., Goldstein, A. H., Hering, S. V., de Gouw, J.,
1052 Baumann, K., Lee, S.-H., Nenes, A., Weber, R. J., and Ng, N. L.: Effects of anthropogenic
1053 emissions on aerosol formation from isoprene and monoterpenes in the southeastern United
1054 States, *Proc. Natl. Acad. Sci. U. S. A.*, **112**, 37-42, [10.1073/pnas.1417609112](https://doi.org/10.1073/pnas.1417609112), 2015.
- 1055 Zanatta, M., Gysel, M., Bukowiecki, N., Müller, T., Weingartner, E., Areskou, H., Fiebig, M., Yttri, K. E.,
1056 Mihalopoulos, N., Kouvarakis, G., Beddows, D., Harrison, R. M., Cavalli, F., Putaud, J. P.,
1057 Spindler, G., Wiedensohler, A., Alastuey, A., Pandolfi, M., Sellegri, K., Swietlicki, E., Jaffrezo, J.
1058 L., Baltensperger, U., and Laj, P.: A European aerosol phenomenology-5: Climatology of black
1059 carbon optical properties at 9 regional background sites across Europe, *Atmos. Environ.*, **145**,
1060 346-364, <https://doi.org/10.1016/j.atmosenv.2016.09.035>, 2016.
- 1061 Zhang, Q., Jimenez, J. L., Canagaratna, M. R., Allan, J. D., Coe, H., Ulbrich, I., Alfarra, M. R., Takami, A.,
1062 Middlebrook, A. M., Sun, Y. L., Dzepina, K., Dunlea, E., Docherty, K., DeCarlo, P. F., Salcedo, D.,
1063 Onasch, T., Jayne, J. T., Miyoshi, T., Shimo, A., Hatakeyama, S., Takegawa, N., Kondo, Y.,
1064 Schneider, J., Drewnick, F., Borrmann, S., Weimer, S., Demerjian, K., Williams, P., Bower, K.,
1065 Bahreini, R., Cottrell, L., Griffin, R. J., Rautiainen, J., Sun, J. Y., Zhang, Y. M., and Worsnop, D. R.:
1066 Ubiquity and dominance of oxygenated species in organic aerosols in anthropogenically-
1067 influenced Northern Hemisphere midlatitudes, *Geophys. Res. Lett.*, **34**,
1068 [doi:10.1029/2007GL029979](https://doi.org/10.1029/2007GL029979), 2007.
- 1069 Zhang, Q., Jimenez, J. L., Canagaratna, M. R., Ulbrich, I. M., Ng, N. L., Worsnop, D. R., and Sun, Y.:
1070 Understanding atmospheric organic aerosols via factor analysis of aerosol mass spectrometry:
1071 a review, *Anal. Bioanal. Chem.*, **401**, 3045-3067, [10.1007/s00216-011-5355-y](https://doi.org/10.1007/s00216-011-5355-y), 2011.
- 1072 Zhang, Y. J., Tang, L. L., Wang, Z., Yu, H. X., Sun, Y. L., Liu, D., Qin, W., Canonaco, F., Prévôt, A. S. H.,
1073 Zhang, H. L., and Zhou, H. C.: Insights into characteristics, sources, and evolution of submicron
1074 aerosols during harvest seasons in the Yangtze River delta region, China, *Atmos. Chem. Phys.*,
1075 **15**, 1331-1349, [10.5194/acp-15-1331-2015](https://doi.org/10.5194/acp-15-1331-2015), 2015.
- 1076 Zhang, Y., Tang, L., Sun, Y., Favez, O., Canonaco, F., Albinet, A., Couvidat, F., Liu, D., Jayne, J. T., Wang,
1077 Z., Croteau, P. L., Canagaratna, M. R., Zhou, H., Prévôt, A. S. H. and Worsnop, D. R.: Limited
1078 formation of isoprene epoxydiols-derived secondary organic aerosol (IEPOX-SOA) under NOx-



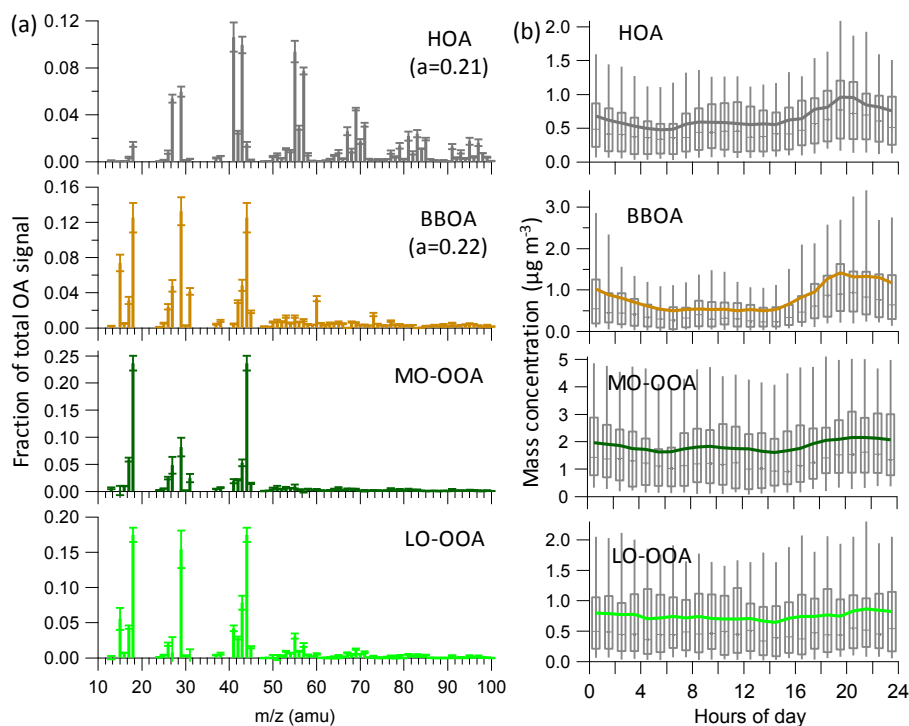
1079 rich environments in Eastern China, *Geophys. Res. Lett.*, 2016GL072368,
1080 doi:10.1002/2016GL072368, 2017.

1081 Zhang, Y., Favez, O., Canonaco, F., Liu, D., Mocnik, G., Amodeo, T., Sciare, J., Prévôt, A. S. H., Gros, V.,
1082 and Albinet, A.: Evidence of major secondary organic aerosol contribution to lensing effect
1083 black carbon absorption enhancement, *npj Climate and Atmospheric Science*, 1, 47,
1084 doi:10.1038/s41612-018-0056-2, 2018.

1085 Zhou, S., Collier, S., Jaffe, D. A., Briggs, N. L., Hee, J., Sedlacek III, A. J., Kleinman, L., Onasch, T. B., and
1086 Zhang, Q.: Regional influence of wildfires on aerosol chemistry in the western US and insights
1087 into atmospheric aging of biomass burning organic aerosol, *Atmos. Chem. Phys.*, 17, 2477-
1088 2493, <https://doi.org/10.5194/acp-17-2477-2017>, 2017.

1089 Zotter, P., Herich, H., Gysel, M., El-Haddad, I., Zhang, Y., Močnik, G., Hüglin, C., Baltensperger, U., Szidat,
1090 S., and Prévôt, A. S. H.: Evaluation of the absorption Ångström exponents for traffic and wood
1091 burning in the Aethalometer-based source apportionment using radiocarbon measurements
1092 of ambient aerosol, *Atmos. Chem. Phys.*, 17, 4229-4249, 10.5194/acp-17-4229-2017, 2017.

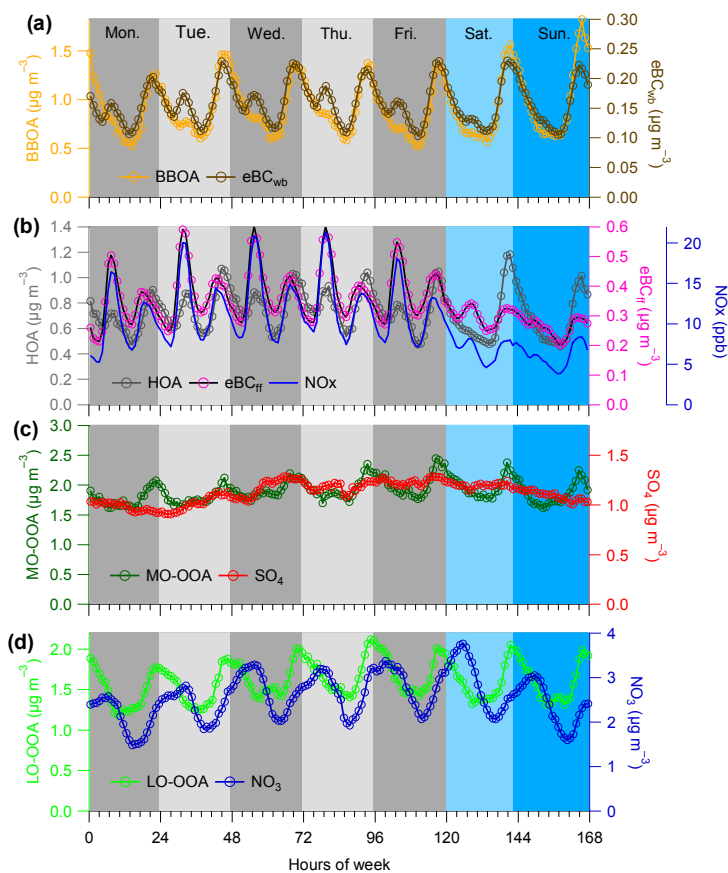
1093
1094



1095

1096 **Figure 1.** Mass spectra (a) and diel variations (b) of four OA factors obtained from the 4-factor
1097 solution of ME-2 runs for winter 2017-2018. In (a), error bars in each plot present 1 standard
1098 deviation. Stick lines indicate average values over all selected ME-2 runs. Averaged a-values
1099 for constrained factors during the ME-2 runs are also shown. In (b), the upper and lower
1100 boundaries of boxes indicate the 75th and 25th percentiles; the vertical lines within the box
1101 correspond to median values; the whiskers above and below boxes refer to 95th and 10th
1102 percentiles; and solid colored lines represent mean values.

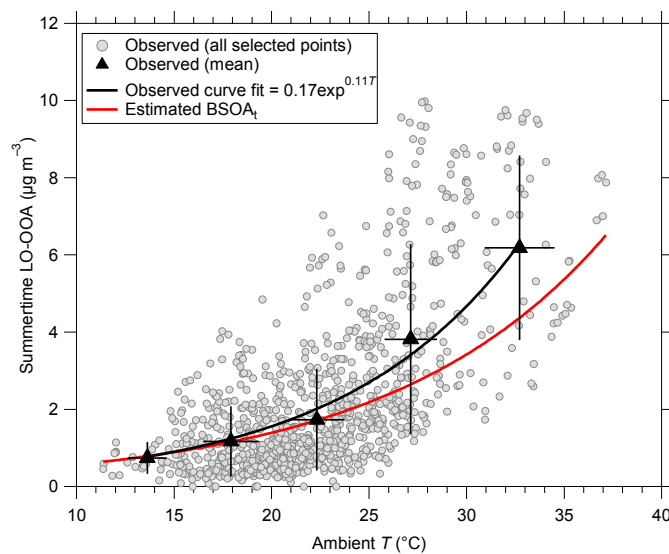
1103



1104

1105 **Figure 2.** Weekly cycles averaged for the entire period of study for (a) HOA, (b) BBOA, (c) MO-
1106 OOA and (d) LO-OOA, along with possible external tracers (eBC_{wb}, eBC_{ff} and NO_x, sulfate, and
1107 nitrate, respectively). Weekdays (24 h) are colored in different gray and weekend days in
1108 different blue.

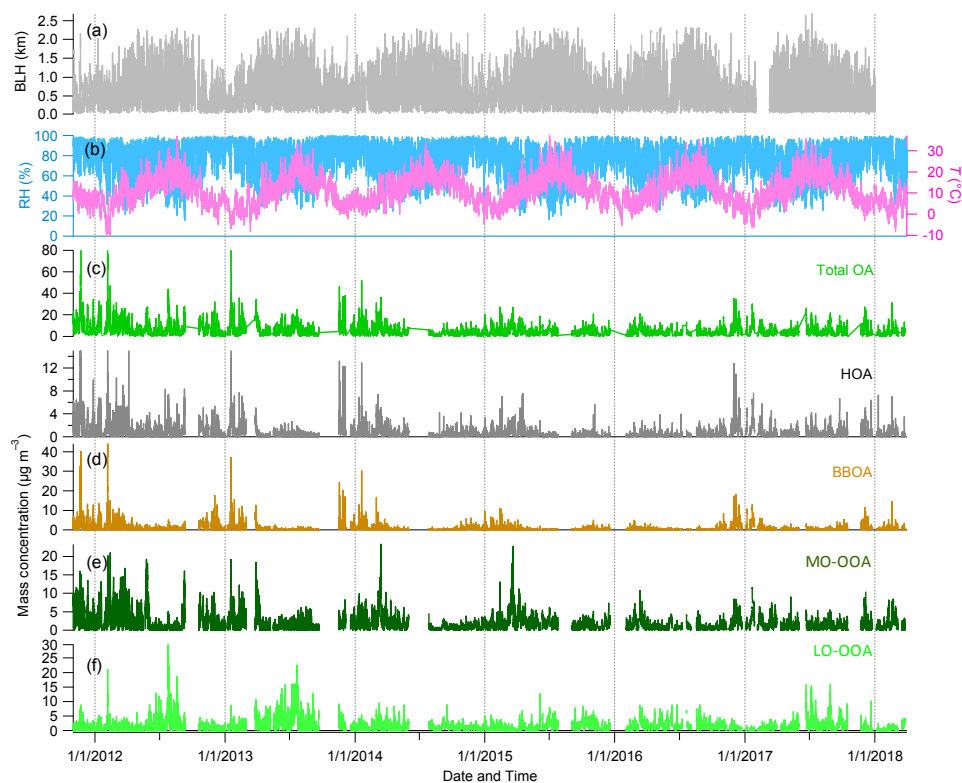
1109



1110

1111 **Figure 3.** Temperature dependence of summertime LO-OOA obtained from observation and
1112 observationally constrained calculation based on biogenic terpene emissions model
1113 (Schurgers et al., 2009; Leaitch et al., 2011).

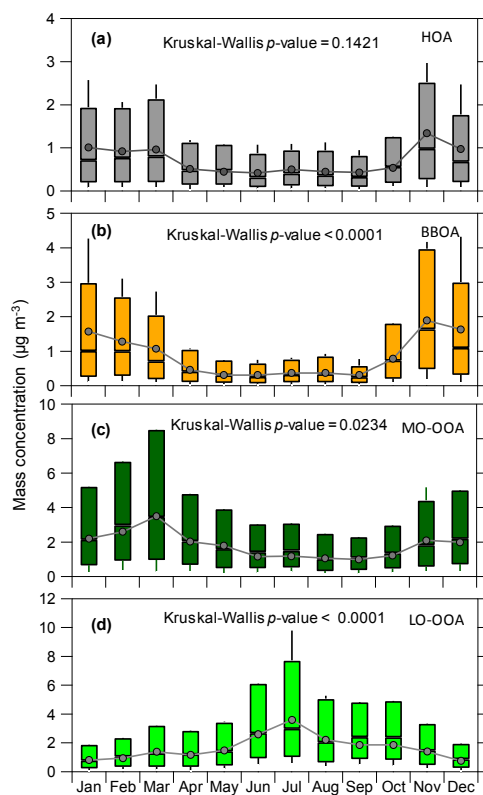
1114



1115

1116 **Figure 4.** 6⁺-year timeseries of meteorological parameters, i.e., (a) boundary layer height (BLH);
1117 and (b) relative humidity (RH) and temperature (*T*), and mass concentrations of (c) total OA
1118 and four OA PMF factors, i.e., (c) HOA, (d) BBOA, (e) MO-OOA, and (f) LO-OOA.

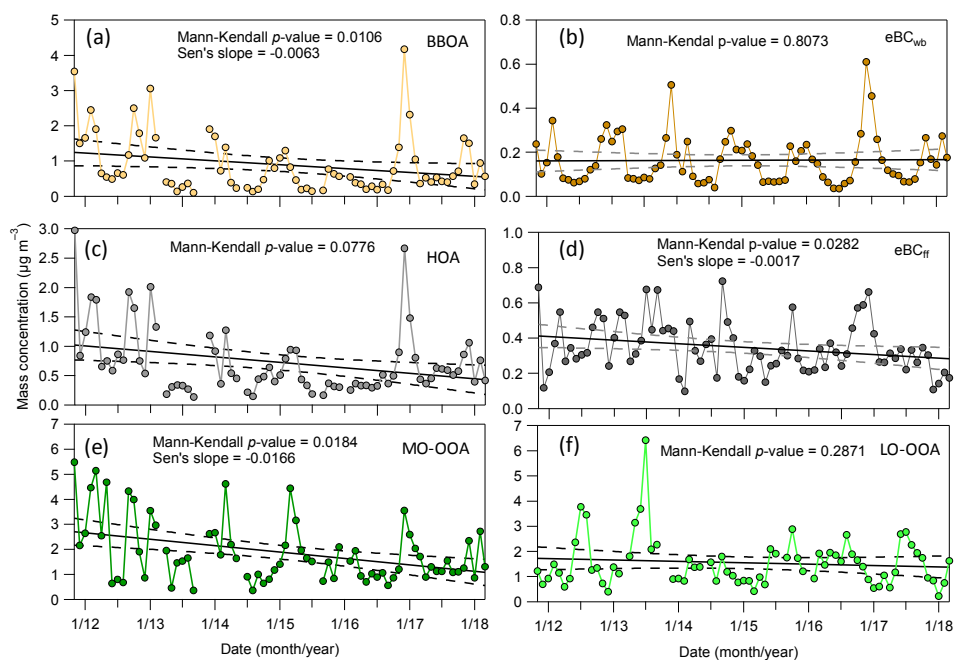
1119



1120

1121 **Figure 5.** Monthly variations of the four OA factors and associated Kruskal-Wallis p -value for
1122 detecting seasonality. The box plots describe the different percentiles (10th, 25th, 50th, 75th,
1123 and 90th) and the mean (gray solid circle).

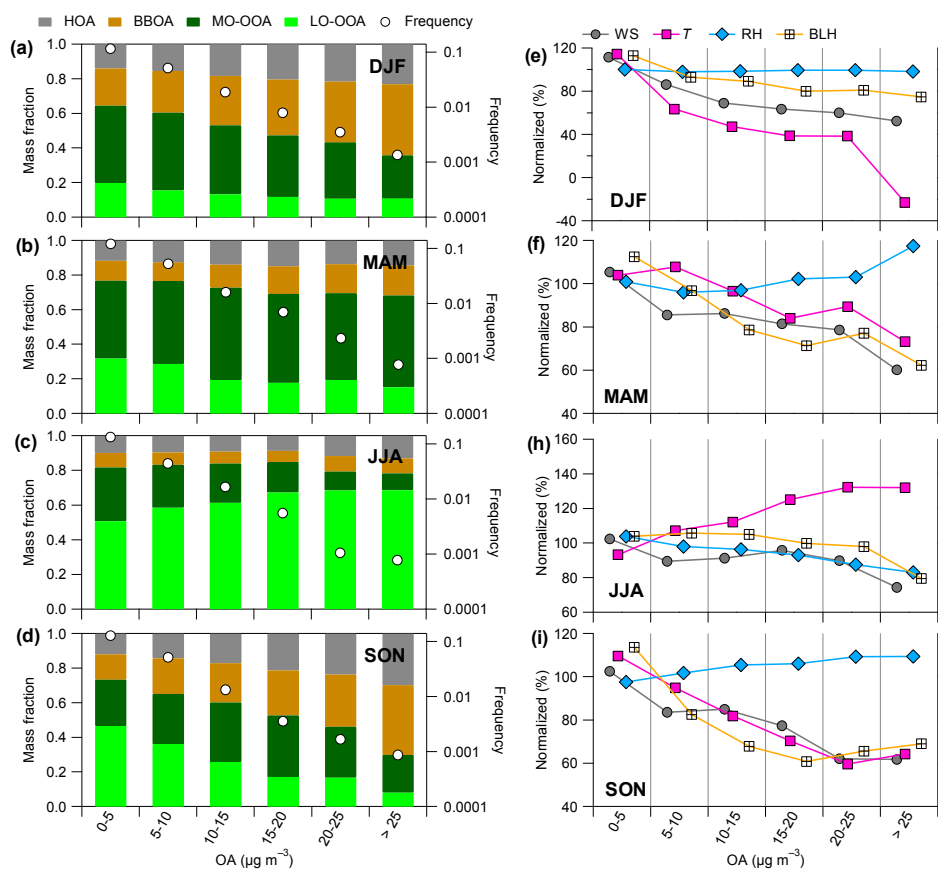
1124



1125

1126 **Figure 6.** 6⁺-year trends of four OA factors. The (seasonal) Mann-Kendall testes associated
1127 with estimated Sen's slope (only given here when trends are assumed significant, i.e., if MK p -
1128 value < 0.05) were used for the trend analysis.

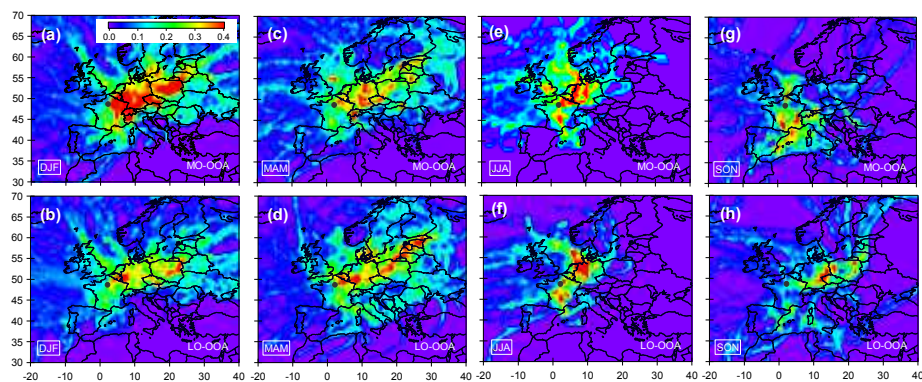
1129



1130

1131 **Figure 7.** (a-d) mass fraction of OA factors and (e-i) meteorological parameters (i.e., WS, T, RH,
 1132 and BLH) as a function of OA mass loadings in four seasons: winter (DJF), spring (MAM),
 1133 summer (JJA), and fall (SON), along with frequency distributions (white circle points). The
 1134 percent change of all meteorological parameters was normalized based on the average values
 1135 over the 6⁺-years period considered here.

1136



1137

1138 **Figure 8.** Maps for potential source origins of regional transports that may contribute to SOA
1139 (including MO-OOA and LO-OOA) burdens at SIRTA. Observed data points with wind speed
1140 (less than 4 m s^{-1}) and in the presence of precipitation events are filtered for the PSCF
1141 calculation. Black solid point in each plot presents the location of the sampling site.